Max-Planck-Institut
für Meteorologie

MAX-PLANCK-GESELLSCHAFT

International Max Planck Research School
on Earth System Modelling

# Factors Controlling the Position of the Inter-Tropical Convergence Zone on an Aquaplanet

Benjamin Möbis

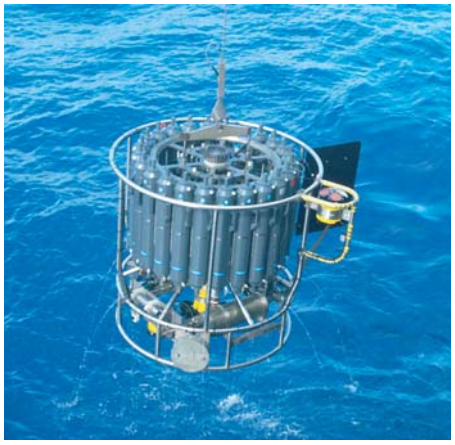

Berichte zur Erdsystemforschung 129/2013

*Reports on Earth System Science*

## Hinweis

Die Berichte zur Erdsystemforschung werden vom Max-Planck-Institut für Meteorologie in Hamburg in unregelmäßiger Abfolge herausgegeben.

Sie enthalten wissenschaftliche und technische Beiträge, inklusive Dissertationen.

Die Beiträge geben nicht notwendigerweise die Auffassung des Instituts wieder.

Die "Berichte zur Erdsystemforschung" führen die vorherigen Reihen "Reports" und "Examensarbeiten" weiter.

## *Notice*

*The Reports on Earth System Science are published by the Max Planck Institute for Meteorology in Hamburg. They appear in irregular intervals.*

*They contain scientific and technical contributions, including Ph. D. theses.*

*The Reports do not necessarily reflect the opinion of the Institute.*

*The "Reports on Earth System Science" continue the former "Reports" and "Examensarbeiten" of the Max Planck Institute.*

## Anschrift / Address

Max-Planck-Institut für Meteorologie
Bundesstrasse 53
20146 Hamburg
Deutschland

Tel.: +49-(0)40-4 11 73-0
Fax: +49-(0)40-4 11 73-298
Web: www.mpimet.mpg.de

## Layout:

Bettina Diallo, PR & Grafik

Titelfotos:
vorne:
Christian Klepp - Jochem Marotzke - Christian Klepp
hinten:
Clotilde Dubois - Christian Klepp - Katsumasa Tanaka

Berichte zur Erdsystemforschung 129/2013

# Factors Controlling the Position of the Inter-Tropical Convergence Zone on an Aquaplanet

Benjamin Möbis

aus Freiburg

Hamburg 2012

*Reports on Earth System Science* 129/2013

ISSN 1614-1199

Benjamin Möbis
Max-Planck-Institut für Meteorologie
Bundesstrasse 53
20146 Hamburg

Als Dissertation angenommen
vom Department Geowissenschaften der Universität Hamburg

auf Grund der Gutachten von
Prof. Dr. Björn Stevens
und
Dr. Marco Giorgetta

Hamburg, den 28. Januar 2013
Prof. Dr. Jürgen Oßenbrügge
Leiter des Departments für Geowissenschaften

ISSN 1614-1199

# Factors Controlling the Position of the Inter-Tropical Convergence Zone on an Aquaplanet

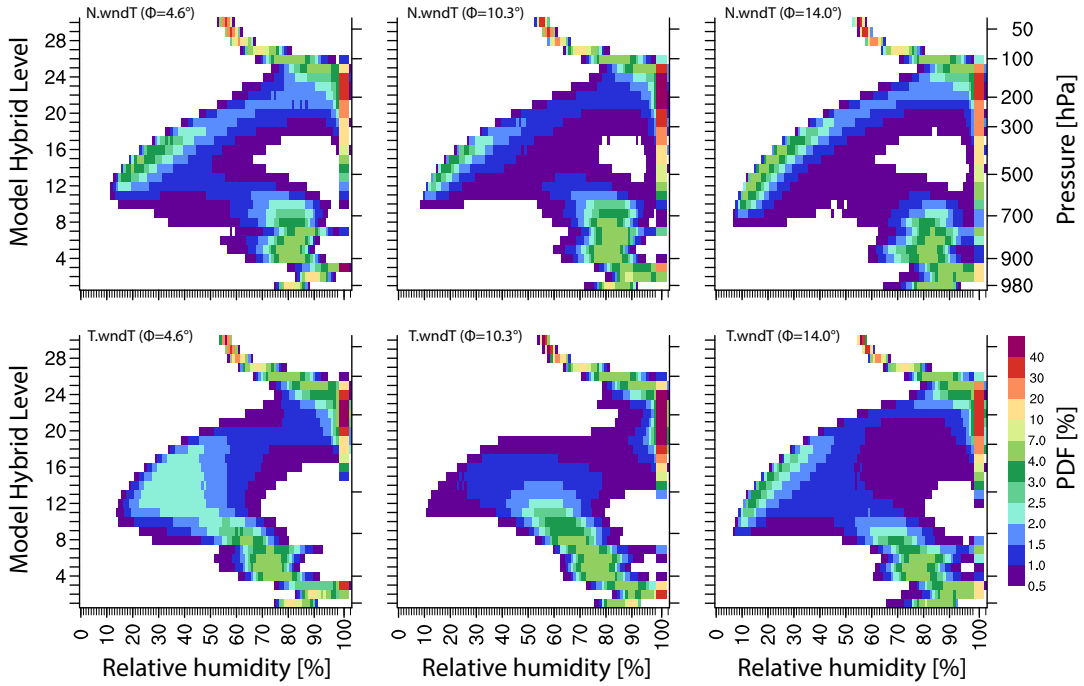


Benjamin Möbis

Hamburg 2012

**Abstract**

Aqua planet experiments performed with fixed sea surface temperatures (SST) using the ECHAM6 GCM are studied to understand properties that influence the position of the inter tropical convergence zone (ITCZ). A single ITCZ develops when using the Nordeng scheme and a double ITCZ when using the Tiedtke scheme. The position of the ITCZ is found to depend on a feedback loop process wherein convective heating drives pressure gradients and winds, which determine the rate of surface evaporation, which influences the boundary layer moist static energy, which finally couples back to the pattern of convective heating. This feedback loop process is sensitive to the SST profile and the choice of the convection scheme. However SSTs are only important in so far as they control the boundary layer moist static energy. The feed-back loop can be broken by specifying the wind used to calculate surface fluxes, in so doing it is possible to control the magnitude of boundary layer moist static energy and hence the position of the ITCZ.

The cloud top height and therefore the convective heating decisively depends on the entrainment rates and the free tropospheric humidity. In the double ITCZ case the humidity in the lower free troposphere is higher on the equatorward side of the double ITCZ compared to the poleward side. Therefore an increase of the entrainment rates favor convection on the equatorward side. This explains why the Nordeng scheme produces a single ITCZ, although the Tiedtke scheme produces a double ITCZ. For this effect the mixing in the upper part of the free troposphere is of minor importance while a sufficient amount of mixing through the whole lower part of the free troposphere is needed.

For the feedback loop to push the ITCZ towards the equator it is decisive to moisten the ITCZ region and to dry other regions. Herewith the humidity mainly depends on the vertical velocity, which itself depends on the sum of convective heating and radiative cooling. For a single ITCZ to form either the water vapor and the cloud radiative effect must lead to a lower radiative cooling rate in the ITCZ than poleward of the ITCZ.

# Contents

# Chapter 1

# Introduction

Most of the coupled climate models participating in the coupled model intercomparison project, phase 3 (Meehl et al. 2007, CMIP3), show some degree of the double ITCZ (inter tropical convergence zone) problem, wherein the ITCZ in the southern hemisphere is too pronounced, and, or, too zonal (Lin 2007). The problem is not well understood, is expressed to differing degrees in different models, and is aggravated when coupled to an ocean model. However, because the problem is also evident when sea surface temperatures are prescribed, at least part of the problem must originate from the atmospheric models. Many aqua planet studies, wherein the land surface is replaced by water and the distribution of sea surface temperatures is prescribed, show a strong dependence of the ITCZ position on the chosen convection parameterization. Some of these models show a single ITCZ for a given distribution of sea surface temperatures, and others show a double ITCZ (e.g. Liu et al. 2009; Hess et al. 1993; Williamson 2012; Oueslati and Bellon 2012; Lee et al. 2003; Chao and Chen 2004). The reason for this dependence is not well understood. Nevertheless the understanding of this dependence is important for the understanding of convective organization in more complex situations.

In this study a comprehensive atmospheric GCM, run with two different convective parameterizations on a aquaplanet, is applied to this problem. The different representations of deep convection have a strong influence on the position of the ITCZ and offer the opportunity to isolate and understand factors controlling its position, at least in ideal circumstances.

There is a large literature about mechanisms determining the ITCZ position. Charney (1971) proposed a moisture convergence mechanism (CISK, or conditional instability of the second kind) where the ITCZ position is governed by a balance between moisture convergence and local surface evaporation. Holton et al. (1971) proposed the Wave CISK mechanism, wherein tropical waves modulate surface convergence and control the position of the ITCZ. Chao and Chen (2001, 2004) interpreted the ITCZ position as a balance between two attractors one associated with the sea surface temperature, which drives local evaporation, and the other with the Coriolis parameter, which is related to Ekman convergence in the boundary layer. Liu et al. (2009) in turn proposed that a single ITCZ is associated with a prevailing CISK mechanism while a

double ITCZ is associated with the wind evaporation feedback. Bellon and Sobel (2010) on the other hand emphasized the influence of the vertical temperature profile and the free tropospheric moisture convection feedback. For most of these mechanisms it is not clear how assumptions that one makes in the parameterization of deep convection influence the ITCZ position.

Differential surface heating does play a central role in creating sea surface temperature gradients for some theories as to what controls the ITCZ position (see Oueslati and Bellon 2012). Lindzen and Nigam (1987) proposed that the sea surface temperature and its gradient control the boundary layer convergence, and thereby the ITCZ position. Although the correlation between sea surface temperature and the ITCZ position is high, it can not fully explain the observed precipitation patterns (Back and Bretherton 2009). Hyashi and Sumi (1986) even showed that a double ITCZ can form with the sea surface temperature maximum at the equator. A high sea surface temperature seems to be a necessary but not sufficient condition for the ITCZ location (Numaguti 1993). Various studies emphasized the influence of the latitudinal variation of surface evaporation through the variation of the zonal wind speed, referred to as the wind evaporation feedback on the ITCZ position (Liu et al. 2009; Chao and Chen 2004; Numaguti 1993; Numaguti and Hayashi 1991). For instance, Numaguti (1993) used an aquaplanet GCM with prescribed sea surface temperatures to demonstrate that if the wind dependence of the surface evaporation scheme is removed, a single ITCZ will occur instead of double ITCZ. So while it is clear that the distribution of low level winds plays an important role in determining the position of the ITCZ, what remains unclear is the relative role of surface moisture convergence versus an evaporative wind feedback mechanism in determining the ITCZ position. The latter issue can, in particular, be difficult to interpret because evaporation acts over the history of the development of the boundary layer in advance of the development of convection; as pointed out by Neelin and Held (1987), the local correlation between evaporation and precipitation is weak, so that the precipitation is rather balanced by moisture convergence than by surface evaporation, at least locally. Because convection also leads to convergence these types of relationships make it difficult to separate ultimate from proximate causes of convection based on observations alone.

There is also much observational support for the influence of lower tropospheric humidity on deep convection (Neelin et al. 2009; Derbyshire et al. 2004). Neelin et al. (2009) showed that entrainment in the lower free troposphere tends to prevent deep convection unless this layer is sufficiently close to saturation and saw the best fit for the"critical column water vapor" to the saturation specific humidity between 550 and 875 hPa. Derbyshire et al. (2004) compared two cloud resolving models with several single column models. Although the cloud resolving models agree well with each other and show a humidity sensitivity close to that observed, the single column models differ in many ways from each other and the observations. Various studies indicate that

representations of convection in models is insufficiently sensitive to the entrainment of moisture in the lower free troposphere (Neelin et al. 2009; Derbyshire et al. 2004; Bechtold et al. 2008; Neale et al. 2008). On the other hand, Tompkins (2001) found that the sensitivity to free tropospheric humidity plays an important role in the organization of tropical deep convection. Oueslati and Bellon (2012) showed that increasing the entrainment parameter leads to an equatorward shift of the ITCZ position.

As reviewed above, there is an extensive literature discussing how large scale features influence the placement of the ITCZ, these features include the distribution of tropical waves, patterns of sea surface temperatures, effects of planetary waves, and the influence of local winds. The literature on how particular assumptions in the design of convection schemes interact with and determine the large scale circulation (even for fixed sea surface temperatures) and thus influence the ITCZ position is less well developed, and are a focus of this study.

The literature on how particular assumptions that are made in designing a convective scheme interact with, and help determine, the large scale circulation (even for fixed sea surface temperatures) to influence the ITCZ position is less well developed, and are a focus of this study.

The remainder of the manuscript is organized as follows: In Chapter 2 the experimental methodology is presented, including an extensive discussion of the convective parameterizations employed, as their differences are not adequately described in the literature. In Chapter 3 the behavior of the GCM for the two representations of convection is explored as a function of the underlying distribution of sea surface temperatures, and the nature of the coupling between the deep convection and the large scale atmosphere circulation is identified. This coupling between the large scale and the deep convection is broken in Chapter 4 and provides an opportunity to study how different assumptions in the convective parameterization respond to given large scale conditions. Based on the results of Chapter 4, Chapter 5 proposes and tests mechanisms controlling the coupling between convection and the large scale circulation. Chapter 6 analyzes the sensitivity of convective organization to the vertical distribution of mixing. Chapter 7 discusses the influence of water vapor and cloud radiative effects on the ITCZ placement and how they are connected to the mechanisms of convective organization discussed in Chapter 5. Conclusions are presented in Chapter 8. Chapter 1, 2 and 8 have been in large parts published in Möbis and Stevens (2012) as well as Chapter 3, 4 and 5 verbatim.

# Chapter 2

# Model and Experiments

## 2.1 Convective Parameterization

For our experiments either the "original" convective parameterization by Tiedtke (1989) was used, which was implemented in ECHAM3, or a variant thereof proposed by Nordeng (1994) which has been standard in all versions of ECHAM since ECHAM4. Hereafter these are referred to as the Tiedtke and Nordeng schemes respectively. Because Nordeng is the default scheme in ECHAM6, ECHAM6 Nordeng is often simply referred as ECHAM6. Since in this thesis the influence of the convection scheme on the ITCZ pattern is analyzed this Section will present the major differences between the Tiedtke and Nordeng scheme as well as some unpublished details of which some turn out to have a decisive influence on the ITCZ pattern. The two convection schemes mainly differ from one another in their formulation of deep convection, specifically the representation of entrainment, detrainment and cloud base mass flux. In what follows the differences between the schemes are documented, and the details of how they have come to be implemented in ECHAM6. Because the implementation differs from what is described in the original publications it is described in more depth here. For the basic background of the mass flux approach adopted in both schemes, however, the reader is referred to the original literature by Arakawa and Schubert (1974) and Tiedtke (1989).

The organizing concept in both the Tiedtke and Nordeng schemes is the mass flux carried by an ensemble of convective elements. The net updraft mass flux is denoted by $M_{\mathrm{up}}$, and its height evolution depends on mass sources and sinks as follows

$$\frac{\partial M_{\mathrm{up}}}{\partial z} = E_{\mathrm{trb}} + E_{\mathrm{org}} - D_{\mathrm{trb}} - D_{\mathrm{org}} \tag{2.1}$$

Equation 2.1 defines the "updraft model", its behavior depends on the chosen form for the mass source and sink terms.

The mass sources are denoted by $E$, for entrainment, and the sinks are denoted by $D$ for detrainment. Two qualitatively different types of mass source and sinks are admitted. The first type is associated with small scale mixing, and is referred to as "turbulent entrainment" or "detrainment", and is modeled as proportional to the mass

flux itself, such that

$$E_{\text{trb}} = \varepsilon_{\text{trb}} M_{\text{up}} \quad \text{and} \quad D_{\text{trb}} = \delta_{\text{trb}} M_{\text{up}} \tag{2.2}$$

The parameters $\delta_{\text{trb}}$ and $\varepsilon_{\text{trb}}$ have the units of an inverse length scale. In both Tiedtke and Nordeng it is assumed that $\delta_{\text{trb}} = \varepsilon_{\text{trb}} = \ell_*^{-1}$ for $p > p_*$. For deep convection $\ell_* = \ell_{\text{d}} = 10\,\text{km}$. For shallow convection $\ell_* = \ell_{\text{s}} = 3.33\,\text{km}$. In the case $\delta = \varepsilon$, turbulent mixing does not change the strength of the updraft mass flux and only influences the intensive quantities of the updraft. At pressures lower than $p_*$, $\varepsilon_{\text{trb}} = 0$ but $\delta_{\text{trb}} = \ell_*^{-1}$, so that in the absence of organized entrainment and detrainment $\partial_z M_{\text{up}} < 0$, the mass flux decreases with height. Hence, $p_*$ defines a "detrainment" level. It is taken as the minimum of two pressure scales,

$$p_* = \begin{cases} \min\left[\frac{1}{2}\left(p_{\text{cb}} + p_{\text{ct}}\right), p_{\text{cb}} - 200\,\text{hPa}\right] & \text{for shallow convection} \\ \min\left[\frac{1}{2}\left(p_{\text{cb}} + p_{\text{ct}}\right), p_{\omega,\text{max}}\right] & \text{for deep convection} \end{cases}, \tag{2.3}$$

which are defined differently depending on whether the convection is determined to be shallow or deep. Here $p_{\text{cb}}$ and $p_{\text{ct}}$ denote the cloud base and cloud top pressures respectively, and $p_{\omega,\text{max}}$ the pressure of the maximum large-scale (environmental) vertical velocity.

In both parameterizations the "organized entrainment" and the "organized detrainment", $E_{\text{org}}$ and $D_{\text{org}}$, are set to zero for shallow convection. For deep convection, using the Tiedtke scheme, the organized entrainment is formulated as follows:

$$E_{\text{org,T}} = \frac{\rho}{q}\frac{\mathrm{d}q}{\mathrm{d}t} \quad \text{for} \quad p > p_*, \tag{2.4}$$

and it is set to zero in the upper ($p \leq p_*$) part of the cloud.

One of the main changes introduced by Nordeng was to parameterize the "organized entrainment" rate for deep convection as a function of the vertically integrated buoyancy of the parameterized updraft $B(z, T_{\text{v,up}})$:

$$E_{\text{org,N}} = M_{\text{up}}\left[\frac{b}{2}\left(w_{\text{cb}}^2 + B(z, T_{\text{v,up}})\right)^{-1} + \frac{1}{\rho}\frac{\mathrm{d}\rho}{\mathrm{d}z}\right] \tag{2.5}$$

where $w_{\text{cb}} = 1\,\text{m s}^{-1}$ is the vertical velocity at cloud base and

$$B(z, T_{\text{v,up}}) = \int_{z_{\text{cb}}}^{z} b(z') \cdot \mathrm{d}z'. \tag{2.6}$$

The buoyancy, $b$, is defined based on the density difference between the updraft and the environment, which can be expressed in terms of state variables as follows:

$$b = g\left[\frac{T_{\text{up}} - T}{T} + \varepsilon_R(q_{\text{up}} - q) - q_{\text{c,up}}\right], \tag{2.7}$$

with $\varepsilon_R = \frac{R_\mathrm{v}}{R_\mathrm{d}} - 1$, $q$ is the water vapor mixing ratio and $q_\mathrm{c}$ the mixing ratio of the water condensate. The variables of the updraft are marked with the subscript "up", the other are those of the environment. This entrainment formulation follows the idea that the cloud covers a constant horizontal area and its positive buoyancy leads to an acceleration of the updraft vertical velocity with an efficiency of 50 %. The resulting vertical divergence of the mass flux is assumed to be balanced by the horizontal convergence of environmental air, which is incorporated into the convective mass flux, i.e., the organized entrainment described by Equation 2.5. This formulation leads to $E_\mathrm{org,N}$ being of the same order of magnitude as $\ell_*^{-1} M_\mathrm{up}$ for any level, which means that $E_\mathrm{org,N}$ is of the same order as $E_\mathrm{trb}$ at levels below $p_*$ where the latter is not forced to vanish.

For deep convection Tiedtke does not explicitly represent organized detraiment, i.e., $D_\mathrm{org,T} = 0$. In the Nordeng parameterization of deep convection a more elaborate approach is taken. This involves the introduction of a new length scale, the "lowest possible organized detrainment level" or $z_\mathrm{low}$. While below $z_\mathrm{low}$ the organized detrainment is zero, above $z_\mathrm{low}$ the organized detrainment is distributed as

$$D_\mathrm{org,N} = M_\mathrm{up} \frac{1}{\sigma} \frac{\partial \sigma}{\partial z} \quad \text{with} \quad \sigma = \sigma_0 \cdot \cos\left( \frac{\pi}{2} \frac{z - z_\mathrm{low}}{z_\mathrm{ct} - z_\mathrm{low}} \right) \tag{2.8}$$

with $z_\mathrm{ct}$ defining the cloud top height and $\sigma$ the horizontal area covered by the updraft. This new length scale, $z_\mathrm{low}$ is defined as the level of neutral buoyancy of a convective updraft with an entrainment rate of $\varepsilon = \frac{1}{2(\gamma + z - z_\mathrm{cb})}$ with $\gamma = b^{-1} w_\mathrm{cb}^2 = 25\,\mathrm{m}$ which corresponds to a vertical velocity at cloud base of $w_\mathrm{cb} = 1\,\mathrm{m\,s^{-1}}$ and an excess buoyancy of 1 K there. This leads to the implicit definition of $z_\mathrm{low}$ (see equation 24 Nordeng 1994):

$$\int_{z_\mathrm{cb}}^{z_\mathrm{low}} \frac{\partial h}{\partial z} \sqrt{\gamma + z - z_\mathrm{cb}} \cdot \mathrm{d}z = 0 \tag{2.9}$$

where $h$ is the moist static energy of the environment. Below the level of neutral buoyancy, air detrained by the organized detrainment term is not detrained with the thermodynamic properties of the updraft, rather it is detrained with the thermodynamic properties of a saturated parcel of air that is neutrally buoyant with respect to the environment. Because the updraft has a positive buoyancy this formulation allows an increase of the updraft moist static energy with height. Although it can be interpreted as a kind of 'unmixing', one must recognize that the convective ensemble is a composite over convective elements with different moist static energies. Because the clouds with the lowest moist static energy are assumed to terminate first the remaining convective elements now have a larger moist static energy than before. To avoid that the updraft has a higher moist static energy than an adiabatic cloud would have, the organized detrainment is limited such that the moist static energy does not increase faster with height than it would if it were to linearly increase to its cloud base value at the height of cloud top (based on the previous estimate of cloud top height).

The cloud top is treated in a separate way, which does not distinguish between the two schemes or convection modes. No entrainment is applied at the level of neutral buoyancy (first half level at which the updraft is not buoyant with respect to the environment) and the updraft mass flux is fully detrained over two levels following the idea of an overshooting plume. In this approach, the mass flux detrained at the level of neutral buoyancy is set to $(1-\beta)\cdot M_{\mathrm{up}}$, and the remainder, $\beta \cdot M_{\mathrm{up}}$, overshoots, and is detrained into the next level. The overshooting fraction $\beta$ is set to the value of 0.21. This approach is also followed by the shallow component of the Tiedtke and Nordeng schemes (which are identical to one another). Because $\beta$ ends up having an important influence on low clouds, it has evolved into an important tuning parameter (Mauritsen et al. 2012).

In the Tiedtke parameterization with deep and shallow convection, and in the Nordeng parameterization with shallow convection, the mass flux evaluated at cloud base, $M_{\mathrm{up}}(z_{\mathrm{cb}})$ is proportional to the moisture convergence within the sub cloud layer, $\dot{Q}(0, z_{\mathrm{cb}})$, as follows:

$$M_{\mathrm{up}}(z_{\mathrm{cb}}) = \frac{\dot{Q}(0, z_{\mathrm{cb}})}{[q_{\mathrm{up}}(z_{\mathrm{cb}}) + q_{\mathrm{c,up}}(z_{\mathrm{cb}}) - 0.3 \cdot q_{\mathrm{dn}}(z_{\mathrm{cb}}) - 0.7 \cdot q(z_{\mathrm{cb}})]}. \tag{2.10}$$

Here

$$\dot{Q}(z_1, z_2) = \int_{z_1}^{z_2} \rho \frac{\mathrm{d}q}{\mathrm{d}t} \mathrm{d}z \tag{2.11}$$

defines the moisture convergence between two levels, $z_1$ and $z_2$.

The proportionality between the cloud base mass flux and the moisture convergence is related by the humidity differences between the updraft, downdraft and environment at cloud base, e.g. Equation 2.10. In the absence of downdrafts, $q_{\mathrm{dn}}(z_{\mathrm{cb}})$ is set equal to the value of $q(z_{\mathrm{cb}})$ for the purposes of computing the cloud base mass flux. Because $T_{\mathrm{up}}$ is required to calculate the downdraft (see 3.b. Tiedtke 1989) and hence $q_{\mathrm{dn}}(z_{\mathrm{cb}})$ as well as $p_{\mathrm{ct}}$ is required to calculate $p_*$ the updraft is first calculated in the absence of downdrafts and with $p_{\mathrm{ct}}$ is set to the adiabatic cloud top height for the purpose of calculating $p_*$. The resulting vertical $T_{\mathrm{up}}$ profile is used to calculate the downdraft. The updraft is then recalculated using the resulting $p_{\mathrm{ct}}$ for the calculation of $p_*$ as well as $q_{\mathrm{dn}}(z_{\mathrm{cb}})$ for calculating the cloud base mass flux. Effectively this defines an iterative procedure, but for reasons of expediency only one iteration is performed.

The other major modification which Nordeng implemented in the Tiedtke scheme is buoyancy closure for deep convection. The Nordeng parameterization determines the mass flux at cloud base through a quasi equilibrium assumption, such that it relaxes the vertical integrated buoyancy $B(z_{\mathrm{ct}}, T_{\mathrm{v,up}})$ to zero with a prescribed decay time, $\tau$:

$$\dot{B}(z_{\mathrm{ct}}, T_{\mathrm{v,up}}) = \frac{B(z_{\mathrm{ct}}, T_{\mathrm{v,up}})}{\tau} \quad \text{with} \quad \tau = 7200\,\mathrm{s} \tag{2.12}$$

where the dot notation denotes differentiation in time. It is assumed that the heating by convection $\dot{B}$ mainly comes from the large scale subsidence, which compensates the convective mass flux such that there is no net vertical mass transport by convection. Thus $\dot{B}$ can be approximated by a function $\mathcal{W}$ which measures the time rate of change of the virtual temperature of the environment. Therefore $\mathcal{W}$ can be related to the environmental lapse rates of dry static energy, $s = c_{\mathrm{p}}T + gz$, and water vapor mixing ratio, $q$, as well as the convective mass flux, $M(z) = M_{\mathrm{up}}(z) + M_{\mathrm{dn}}(z)$ as follows :

$$\begin{aligned}\dot{B}(z_{\mathrm{ct}}, T_{\mathrm{v,up}}) = \mathcal{W}(z_{\mathrm{ct}}, M) &= -\int_{z_{\mathrm{cb}}}^{z_{\mathrm{ct}}} \frac{g}{T_{\mathrm{v}}} \frac{\partial T_{\mathrm{v}}}{\partial t} \mathrm{d}z \\ &= -\int_{z_{\mathrm{cb}}}^{z_{\mathrm{ct}}} \left( \frac{1}{c_{\mathrm{p}} T} \frac{\partial s}{\partial z} + \varepsilon_R \frac{\partial q}{\partial z} \right) \frac{g}{\rho} M \, \mathrm{d}z.\end{aligned} \tag{2.13}$$

Here the downdraft mass flux is given by the downdraft model, and depends on the updraft properties and height as well as the environmental conditions.

Rather than directly solving Equation 2.13, which is implicit in $M_{\mathrm{up}}(z_{\mathrm{cb}})$, the Nordeng scheme takes an approximate approach using a truncated iterative procedure. It does so by initializing the updraft mass flux with the cloud base value $\hat{M}_{\mathrm{up}}(z_{\mathrm{cb}})$, defined to equal the Tiedtke closure in the absence of downdrafts. Further $p_{\mathrm{ct}}$ is set to the adiabatic cloud top height for the purpose of calculating $p_*$. From this, an updraft can be calculated given $\hat{z}_{\mathrm{ct}}$, $\hat{M}_{\mathrm{up}}$ and $\hat{T}_{\mathrm{v,up}}$. $\hat{T}_{\mathrm{v,up}}$ and $\hat{M}_{\mathrm{up}}(z_{\mathrm{cb}})$ are used to calculate the downdraft, $\hat{M}_{\mathrm{dn}}$. By assuming that $B(z_{\mathrm{ct}}, T_{\mathrm{v,up}}) = B(\hat{z}_{\mathrm{ct}}, \hat{T}_{\mathrm{v,up}})$ and

$$\mathcal{W}(z_{\mathrm{ct}}, M) = \frac{M_{\mathrm{up}}(z_{\mathrm{cb}})}{\hat{M}_{\mathrm{up}}(z_{\mathrm{cb}})} \mathcal{W}(\hat{z}_{\mathrm{ct}}, \hat{M}). \tag{2.14}$$

one arrives at and explicit equation for the cloud base mass flux, namely

$$M_{\mathrm{up}}(z_{\mathrm{cb}}) = \frac{\hat{M}_{\mathrm{up}}(z_{\mathrm{cb}}) \cdot B(\hat{z}_{\mathrm{ct}}, \hat{T}_{\mathrm{v,up}})}{\tau \cdot \mathcal{W}(\hat{z}_{\mathrm{ct}}, \hat{M})} \tag{2.15}$$

With $M_{\mathrm{up}}(z_{\mathrm{cb}})$ and using $\hat{z}_{\mathrm{ct}}$ for the calculation of $p_*$ the final updraft can now be calculated.

Although Tiedtke and Nordeng differ in their closure, and elements of the cloud model, the trigger of the convection scheme is identical. In both schemes, convection is triggered if three conditions are met:
(i) the moisture convergence must be positive

$$\dot{Q}(0, z_{\mathrm{cb}}) > 0; \tag{2.16}$$

(ii) the updraft humidity at cloud base must be more than 1% higher than the humidity of the environment

$$q_{\mathrm{up}}(z_{\mathrm{cb}}) + q_{\mathrm{c,up}}(z_{\mathrm{cb}}) > 1.01 \cdot q(z_{\mathrm{cb}}); \tag{2.17}$$

(iii) the updraft must be positively buoyant with respect to the environment; where the updraft properties include a perturbation associated with the standard deviation of the temperature $\sigma_T$ at the lowest model level

$$T_{\mathrm{up}}\left(1+\varepsilon_R \cdot q_{\mathrm{up}} - q_{\mathrm{c,up}}\right) + \sigma_T > T(1+\varepsilon_R q) \quad \text{for} \quad z \leq z_{\mathrm{cb}}. \tag{2.18}$$

The type of convection is determined through the strength of the moisture convergence, such that if the moisture convergence exceeds the surface evaporation by more than 10 %

$$\dot{Q}(0,\infty) > 1.1 \cdot \left.\overline{w'q'}\right|_{\mathrm{srf}}, \tag{2.19}$$

deep convection is triggered. If the cloud depth is less than or equal to 200 hPa in the first updraft calculation by the deep convection scheme then deep convection is determined to have been unsuccessful and the final iteration step is performed using the shallow updraft mode.

In the Tiedtke parameterization, the method of solving for the updraft height introduces an unfortunate side effect. This side effect arises because of the $p_*$ formulation in the mixing rules, wherein $p_*$ depends on $p_{\mathrm{ct}}$ (see Equation 2.3). In the initial calculation of the updraft $p_{\mathrm{ct}}$ is set to the adiabatic cloud top height. This the lower bound on $p_*$ and thus allows the initial updraft to mix over a large part of its depth, which often leads to a much lower estimate for the cloud top height in the initial updraft compared to the adiabatic $p_{\mathrm{ct}}$. The subsequent (or final) updraft then evolves with a much larger value of $p_{\mathrm{ct}}$, and hence reaches the depth $p_*$, where entrainment is turned off, at a lower altitude. Because entrainment is set to zero at pressures lower than $p_*$ the final updraft can become, in turn, much deeper. This inconsistency, essentially an overshoot in the truncated iteration based solution for the updraft height, has the effect of causing the scheme to produce higher cloud tops in drier atmospheres, which is unphysical. In the Nordeng parameterization the cloud top height in the final updraft calculation is limited by the cloud top height of the initial updraft, thereby avoiding this inconsistency. This implementation detail has a large effect on the difference in the behavior of the two schemes.

In summary, the Tiedtke and Nordeng parameterizations differ in their representation of deep convection. Tiedtke parameterizes the cloud base mass flux and the organized entrainment proportional to the moisture convergence and the organized detrainment is limited to the cloud top level. The Nordeng parameterization for deep convection sets the cloud base mass flux using a quasi equilibrium assumption for the convective instability of the free troposphere. Similarly the organized entrainment is based on the updraft buoyancy and the organized detrainment starts from the so called “lowest possible level of organized detrainment” and scales with a height dependent function. Both schemes share a moisture convergence trigger, and an identical representation of shallow convection. These similarities and differences, including the unusual response

of the Tiedtke scheme to a dry atmosphere, should be kept in mind when evaluating the response of the schemes to differences in the large scale environment, as discussed in the remainder of this paper.

## 2.2 Experiments

In this section the general experimental configuration is described as well as the setup of all performed experiments.

All experiments are conducted using the ECHAM6 atmospheric general circulation model as described in Stevens et al. (2012), with boundary conditions and forcings based on the specification by Neale and Hoskins (2001). The surface is set to be water covered with a surface temperature, $T_\mathrm{s}$ prescribed as a function of latitude, $\phi$, such that

$$T_\mathrm{s}(\phi) = T_\mathrm{min} + \Delta T f(\phi;\eta) \tag{2.20}$$

with $T_\mathrm{min} = 273.15\,\mathrm{K}$ and $\Delta T = 27\,\mathrm{K}$ and the shape function, $f$, depending on the latitude and the shape parameter, $\eta$, such that

$$f(\phi;\eta) = \begin{cases} 1 - \eta \sin^2\left(\frac{3\phi}{2}\right) - (1-\eta)\sin^4\left(\frac{3\phi}{2}\right) & \text{for } |\phi| \leq \frac{\pi}{3} \\ 0 & \text{otherwise} \end{cases} \tag{2.21}$$

A variety of different values of $\eta$ were employed (see Table 2.2). $\eta = 1/2$, is referred to as "Qobs" because it is closest to the observed annual and zonal mean sea surface temperature distribution. The sea surface temperature distributions for $\eta = 0$, $1/2$ and 1 are shown in Figure 2.1. Near the equator, where $\phi$ is small, the sea surface temperature gradient is

$$\frac{\mathrm{d}T_\mathrm{s}}{\mathrm{d}\phi} = -\frac{9}{2}\Delta T\left(\eta\phi + \frac{9}{2}(1-\eta)\phi^3\right) \tag{2.22}$$

and thus, for a given $\phi$, increase in magnitude (for small $\phi$) with increasing $\eta$. For this reason the sea surface temperature distribution with $\eta = 0$ is called "flat" by Neale and Hoskins (2001) and the distribution with $\eta = 1$ is called "control." These names are also adopted in the present study. For reference, at $\phi = 10°$ where an ITCZ is frequently observed in the double ITCZ experiments, the SST gradient takes on values of -0.51$\Delta T$, -0.27$\Delta T$ and -0.03$\Delta T$ K rad$^{-1}$ for the control, Qobs and flat experiments respectively. In all the experiments sea ice as well as the orography are set to zero. For the treatment of radiation permanent equinox conditions with a daily solar cycle are enforced, no aerosols are present, and the ozone is specified as described by Williamson (2012).

Experiments show that the results reach a quasi equilibrium after roughly 200 days, and that internal variability on timescales longer than 1000 days is negligible, similar

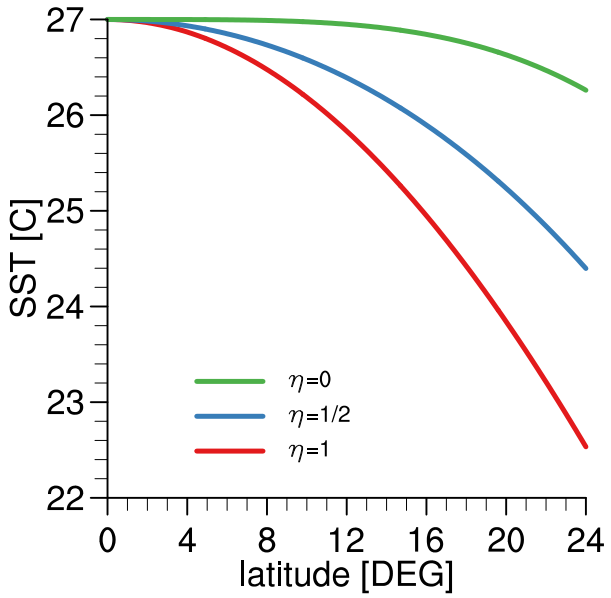


Figure 2.1: Sea surface temperature profiles for $\eta = 0$, $1/2$ and $1$.

to what was found by Medeiros et al. (2008). This then defines our analysis window as the last 1000 days of a 1600 day experiment.

| Name | SST | Convective Scheme | Near Surface Winds |
|---|---|---|---|
| LS | Qobs | None | Interactive |
| N.std | Qobs | Nordeng | Interactive |
| T.std | Qobs | Tiedtke | Interactive |
| N.wndN | Qobs | Nordeng | Climatology from N.std |
| N.wndT | Qobs | Nordeng | Climatology from T.std |
| T.wndN | Qobs | Tiedtke | Climatology from N.std |
| T.wndT | Qobs | Tiedtke | Climatology from T.std |

Table 2.1: The near surface winds refer to the winds that the surface exchange scheme believes are located at the lowest model level, which are used in the surface exchange calculation.

Williamson (2008) pointed out that the horizontal resolution of the model can influence the structure of the simulated ITCZ. In the NCAR model the ITCZ pattern only begins to converge for resolutions higher than T85. Tests with ECHAM6 were

performed using three horizontal resolutions, T31, T63 and T127. For a given convection scheme all three resolutions show qualitatively the same results. Although T31 resolution shows a less peaked single ITCZ with a weaker maximum. Therefore, it is assumed that a horizontal truncation of T63 is sufficient and our subsequent analysis is based on the T63L47 resolution version of ECHAM6.

Table 2.1 summarizes the core set of experiments. Meridional gradients in the sea surface temperature near the equator strongly influence the structure of the ITCZ simulated by ECHAM6. Most of the focus in this paper is on the simulations with the "Qobs" sea surface temperature profile, using either the Tiedtke or Nordeng parameterization, as well as sensitivity studies in which the surface wind speed is fixed in the computation of surface fluxes to some specified climatology. One experiment, called "LS" or large scale, employs no convective parameterization whatsoever. These core experiments are supplemented by sensitivity studies in which the underlying sea surface temperatures are changed, for instance to the "flat" or "control" specifications, or the convection scheme, or the environment it experiences, is varied in some fashion.

| Identifier | Modification | Parameter |
|---|---|---|
| N.$\eta$nn | Different SST | $\eta = \text{nn} = 0, 0.1, 0.2, ...1$ |
| N.031 | Horizontal Resolution | T031 |
| N.127 | ” | T127 |
| N.wnd05 | Surface-flux active wind | 5 $\text{ms}^{-1}$ |
| N.wnd10 | ” | 10 $\text{ms}^{-1}$ |
| N.wnd15 | ” | 15 $\text{ms}^{-1}$ |
| N.wnd10T4x | ” | 4 $\text{ms}^{-1}$ for $\lvert\phi\rvert \leq x$, 10 $\text{ms}^{-1}$ elsewhere |
| N.Tcbm | Cloud base mass flux as in Tiedtke | |
| N.tea | Turbulent entrainment always calculated with the adiabatic cloud top | |
| N.deep | First updraft calculation always uses deep convection when $\lvert\phi\rvert \leq 20°$ | |
| N.rh100 | humidity seen by the convection scheme is set to RH=100% for levels 6-29 (approximately 800 to 50 hPa) and $\lvert\phi\rvert \leq 20°$ | |

Table 2.2: In addition to the experiments listed here, each of which started from the N.std configuration in the base experiment, additional experiments were performed with Tiedtke convection scheme (or the climatology from the other convection scheme, i.e., T.Ncbm is the counterpart to N.Tcbm below).

Although not discussed in detail here a great number of additional experiments were also performed. The purpose of these experiments, outlined in Table 2.2 and described

further below, is to help test ideas that were being developed. For instance the aforementioned tests of horizontal resolution were facilitated by four additional experiments (N.031, N.127, T.031 and T.127). To evaluate whether the different ITCZ patterns of N.std and T.std results from the different mixing or from the different calculation of cloud base mass flux, both experiments were modified by exchanging the calculation of cloud base mass flux, i.e., Experiment N.Tcbm and its counterpart T.Ncbm in Table 2.2. The influence of the trigger between deep and shallow convection was explored by always using deep convection for the first updraft calculation in the tropical region (N.deep and T.deep). It was observed that the cloud top height used for the calculation of turbulent entrainment in the final updraft calculation has a major influence on the ITCZ pattern. To explore this effect more systematically experiments were performed using the adiabatic cloud top height also for the calculation of turbulent entrainment in the final updraft calculation (N.tea and T.tea). An additional experiment (not listed in Table 2.2) using the Tiedtke parameterization was performed, but in which which the cloud top height in the final updraft calculation is limited by the actual cloud top height of the first updraft calculation, as in the Nordeng parameterization. This experiment is named "T.toplimit".

| Identifier | Modification |
|---|---|
| Lat1 | water vapor profile as the 0.93 degree gridpoint in N.std |
| Lat14 | water vapor profile as the 14 degree gridpoint in N.std |
| Lat1/14 | water vapor profile as in Lat1 for the first three gridpoints from the equator and as in Lat14 for the rest |
| q50% | water vapor is multiplied with 0.5 |
| q200% | water vapor is multiplied with 2 |
| 0% CL$n$ | cloudcover is set to 0% for the CL$n$ cloud levels |
| 100% CL$n$ | cloudcover is set to 100% for the CL$n$ cloud levels |
| 2* CL$n$ | cloud ice and liquid is multiplied with 2 for the CL$n$ cloud levels |

Table 2.3: Experiments with the setup of N.std but with modified input to the radiative transfer scheme.

Because the stability and humidity of the free troposphere plays a major role for the ITCZ pattern, additional experiments were performed in which the temperature, geopotential and relative humidity that are seen by the convective parameterization in the tropics were prescribed by a climatology over model hybrid levels 6 through 29 (approximately between 800 and 50 hPa), where level 6 was chose as the lowest level to

exclude the subcloud layer and the first two or three levels of the cloud layer. The relative humidity was set to 100 % because the humidity variability has a major influence on the convection in the Nordeng scheme. The climatological values for the geopotential and temperature were taken from either the N.wndN or N.wndT experiments for the forcing experiments with the Nordeng scheme and from the T.wndN or T.wndT experiments for the forcing experiments with the Tiedtke scheme. Experiments where only the relative humidity was prescribed to 100 % were also performed (Table 2.2).

| Identifier | Mixing constant |
|---|---|
| $\mu$ | $\mu \in \{1.5, 2, 2.5, 3\} \cdot 10^{-4}\mathrm{m}^{-1}$ |
| $\mu$ L12 | $\mu \in \{1.5, 2, 2.5, 3\} \cdot 10^{-4}\mathrm{m}^{-1}$ for the model level 1 to 12 and $\mu = 0$ for the rest |
| 2.0E-4 L12 L$n$=$\mu$ | like 2.0E-4 L12 but $\mu \in \{3, 4, 5\} \cdot 10^{-4}\mathrm{m}^{-1}$ for model level $n$ |
| 2.5E-4 L12 L$n$=$\mu$ | like 2.5E-4 L12 but $\mu \in \{1.5, 0.5\} \cdot 10^{-4}\mathrm{m}^{-1}$ for model level $n$ |
| $\mu = c \cdot (r - \mathrm{Rh})$ | mixing constant $\mu$ depends on relative humidity Rh. $c \in \{3, 6, 9, 12\} \cdot 10^{-4}\mathrm{m}^{-1}$ for $r = 1.1$ and $c \in \{3, 4, 5, 6\} \cdot 10^{-4}\mathrm{m}^{-1}$ for $r = 1.3$ |

Table 2.4: Experiments with a special setup of the Tiedtke scheme (see Chapter 6) which uses a prescribed height dependent mixing constant $\mu$.

The influence of the water vapor and cloud radiative effect on the ITCZ placement is explored with experiments with the setup of the N.std experiment but with modifications to the input of water vapor, liquid and ice as well as cloud cover to the radiative transfer scheme. These experiments are listed in Table 2.3.

A detailed analysis on the connection between updraft mixing and ITCZ placement is done with experiments utilizing an idealized setup of the Tiedtke scheme which does not distinguish between deep and shallow convection and in which the mixing fully depends on a prescribed model level dependent mixing constant. These experiments are listed in Table 2.4.

# Chapter 3

# Large Scale Controls on the Structure of the ITCZ

Experiments with ECHAM6 reproduce the diversity of solutions evident in the aqua planet experiment multi model ensemble (APE-MME) as described by Williamson (2012). For large values of $\eta$ (See Equation 2.21) which lead to a large meridional SST gradient close to the equator both ECHAM6 and ECHAM6 Tiedtke produce a single equatorial ITCZ. As $\eta$ becomes smaller, and the gradients of near equatorial SST become flatter, both versions of the model develop an increasingly off equatorial ITCZ; but they differ in terms of how poleward they place the ITCZ, and at which value of $\eta$ the ITCZ begins to move off the equator (e.g., Figure 3.1). For the "Qobs" case the differences are the most pronounced. Simulations with the Nordeng parameterization are characterized by a single ITCZ, and those with the Tiedtke parameterization have a clear off equatorial double ITCZ (see also Figure 3.2). Also in the APE-MME a double ITCZ predominates in the "flat" ($\eta = 0$) simulations, and a single ITCZ predominates in the "control" ($\eta = 1$) simulations. With the "Qobs" sea surface temperature configuration the picture is more mixed: some models show single while others show a double ITCZ. For example, CCAM-05e and MRI-06 (reproduced from the APE Atlas in Figure 3.3) have the precipitation concentrated within five degrees of the equator comparable to the N.std experiment (Figure 3.2). NCAR-03a and ECMWF-05a (Figure 3.3) show a double ITCZ with the precipitation maxima located about eight degrees poleward of the equator, comparable to the T.std experiment (Figure 3.2). The strongly peaked single ITCZ from DWD-GME-05a (Figure 3.3) is comparable to the LS experiment (Figure 3.2), even though DWD-GME-05a uses a convective parameterization. The ECHAM6 experiments suggest that differences in the ITCZ placement within the APE-MME is caused by differences in the convection schemes employed by the participating models (see also Hess et al. 1993, for further evidence of this point).

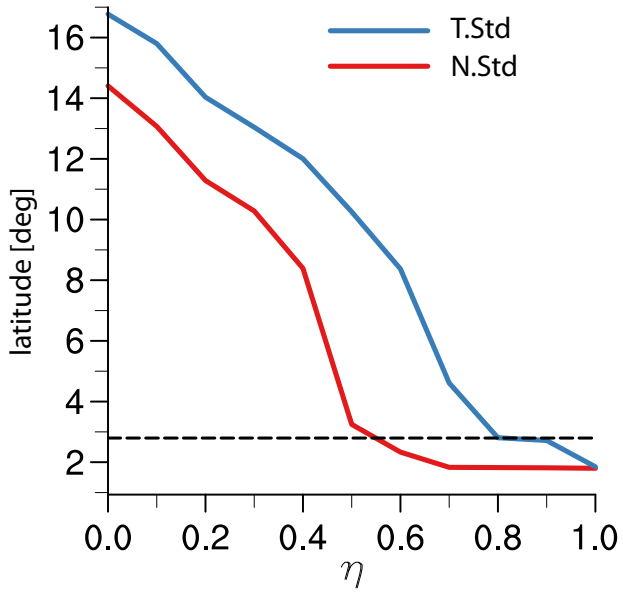


Figure 3.1: Position of the ITCZ as a function of $\eta$ for aqua planet simulations using the Nordeng and Tiedtke convection schemes. The experiment called "Qobs" corresponds to the case where $\eta = 0.5$ for which the difference in the position of the ITCZ is a maximum. The dashed line marks the latitude at which the peaks of the double ITCZ continuously fuse to a single ITCZ.

## 3.1 The ITCZ Position as Part of a Coupled System

The ITCZ position expresses the coupling between the large scale circulation, and the convective dynamics. Convection responds to the development of convective instability, i.e., the destabilization of the atmosphere that results from the extraction of energy out of the free troposphere (by radiative processes) and the input of energy into the boundary layer (through surface fluxes). But the resulting convective heating also modifies the large scale circulation: its effect on the vertical motion modifies the gross moist stability (Neelin and Held 1987; Raymond et al. 2009); its effect on large scale temperature gradients can modify patterns of winds and hence, through surface fluxes, the distribution of boundary layer moist static energy (Neelin and Held 1987; Emanuel 1987); these in turn modify the distribution of convective heating. The experiments show that details of how the convection responds to large scale forcing, and projects back onto the large scale flow, can have a decisive effect on the placement of the ITCZ, as well as patterns and variability of precipitation more generally.

To understand this coupled system it proves useful to ask what controls the maximum in boundary layer moist static energy, $h_{\mathrm{PBL}}$. The question arises from the observation

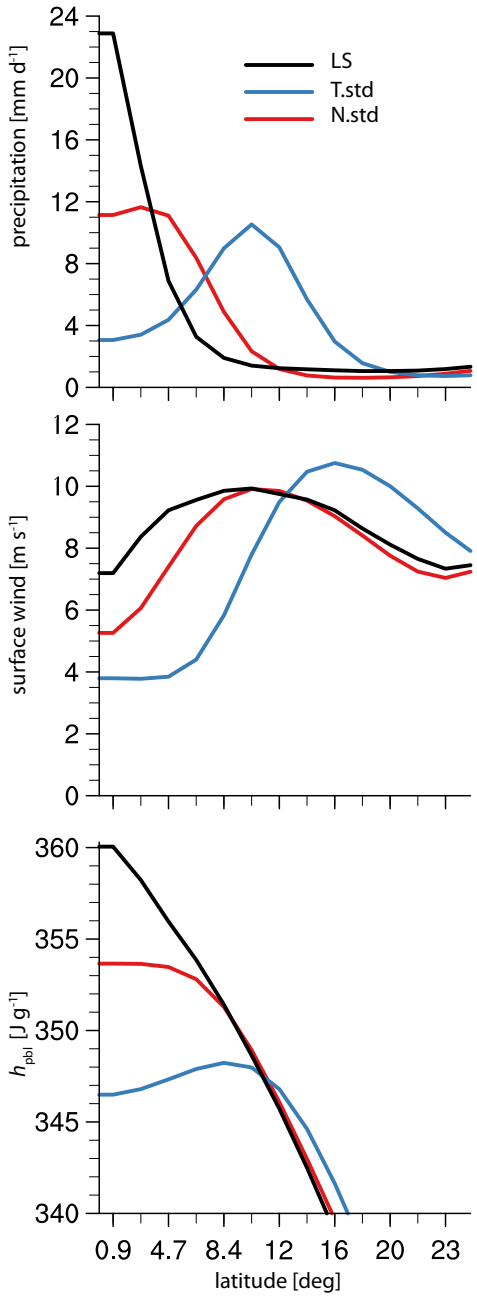


Figure 3.2: Time and zonal average precipitation, surface level horizontal wind and moist static energy in the planetary boundary layer for the experiments LS, T.std and N.std.

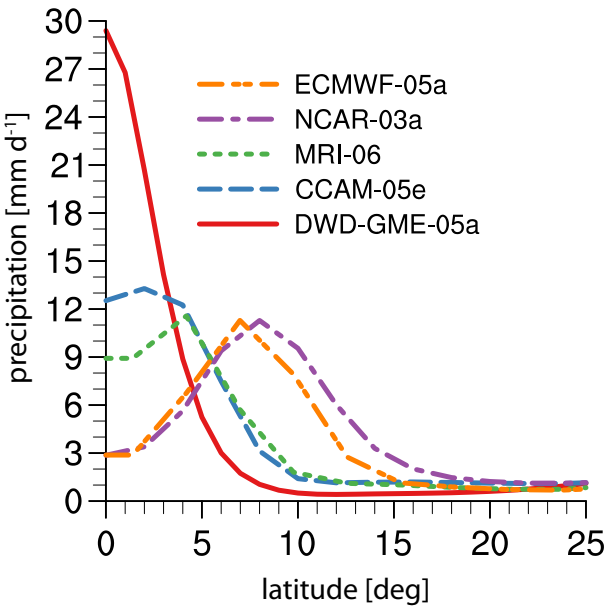


Figure 3.3: Time and zonal average precipitation of five models with Qobs-SST ($\eta = 1/2$) from Williamson (2012).

that both the simulations with Tiedtke and Nordeng locate the ITCZ near the point of maximum $h_{\mathrm{PBL}}$, e.g., Figure 3.2, but is also central to the ideas of boundary layer quasi equilibrium (e.g. Raymond et al. 2003; Sobel and Neelin 2006). From the way the schemes are constructed it is not obvious why this needs to be the case. Because gravity waves are effective in homogenizing the thermal structure of the free troposphere, within the tropics $h_{\mathrm{PBL}}$ determines the amount of energy available to support convection (Emanuel et al. 1994). This explains why the Nordeng scheme, which is based on a CAPE closure, prefers to locate the convection in regions where $h_{\mathrm{PBL}}$ is largest. But, for a given updraft model, the depth of convection mainly depends on $h_{\mathrm{PBL}}$, and this in turn determines the efficiency of convective heating (through its impact on precipitation production and cloud radiative effects) and hence the moisture convergence that drives the Tiedtke closure. So although the Tiedtke scheme only feels $h_{\mathrm{PBL}}$ through the updraft model, in contrast to Nordeng which additionally depends on $h_{\mathrm{PBL}}$ through the closure, for a given state of the free troposphere both can be expected to favor convection in regions where $h_{\mathrm{PBL}}$ maximizes (see also Prive and Plumb 2007, for a discussion of these points).

The distribution of $h_{\mathrm{PBL}}$ is strongly related to the surface winds and the surface value of moist static energy. This can be illustrated by noting that in stationarity $h_{\mathrm{PBL}}$ can be expressed as a balance between surface fluxes which act to relax $h_{\mathrm{PBL}}$ to its surface value, $h_{\mathrm{sfc}}$, and entrainment mixing which relaxes $h_{\mathrm{PBL}}$ to a value, $h_{\mathrm{ft}}$, characteristic of

the free troposphere. In the presence of a constant sink from radiative and advective processes, $\Delta F$, Stevens (2006) showed that this balance takes the form

$$h_{\mathrm{PBL}} = \frac{V h_{\mathrm{sfc}} + E h_{\mathrm{ft}} - \Delta F}{V + E}, \tag{3.1}$$

Here $V$ is an effective exchange velocity at the surface, and is proportional to the windspeed. $E$ measures the entrainment velocity at the top of the boundary layer and is of the same order of magnitude as $V$. From the perspective of this simple balance, with radiative and free tropospheric sinks of $h$ held constant,

$$\delta h_{\mathrm{PBL}} = \alpha_h \delta h_{\mathrm{sfc}} + \alpha_V \delta V, \tag{3.2}$$

where the coefficients,

$$\alpha_h = \frac{V}{V + E} \quad \text{and} \quad \alpha_V = \frac{(h_{\mathrm{sfc}} - h_{\mathrm{ft}})E + \Delta F}{(V + E)^2} \tag{3.3}$$

are both positive. Equation 3.1 identifies how both changes in the surface moist static energy and the wind contribute separately to changes in $h_{\mathrm{PBL}}$, and how other factors work to modify these changes, for instance $h_{\mathrm{ft}}$.

Because $h_{\mathrm{sfc}}$ is a strictly increasing function of $T_{\mathrm{s}}$, which is strictly decreasing with latitude (for $|\phi| < \pi/3$), $h_{\mathrm{PBL}}$ will maximize where $\partial_\phi h_{\mathrm{sfc}} = -\partial_\phi V(\alpha_V/\alpha_h)$. Hence, assuming that the near surface winds are well behaved, so that they increase in the poleward direction as one crosses the ITCZ, $h_{\mathrm{PBL}}$ will maximize at the latitude where $\partial_\phi h_{\mathrm{sfc}}$ first becomes sufficiently large. How large this has to be depends on the convection scheme, through its influence on the mean state, and hence $\partial_\phi V$, $\alpha_h$ and $\alpha_V$.

The above reasoning is based on the expectation that a poleward perturbation in the position of deep convection will act to reduce equatorial surface winds (both by shifting zonal heating, or pressure gradients that support surface easterlies, but also through a poleward shift of the eddy fluxes that mix momentum equatorward). It implies the existence of a feedback loop wherein the ITCZ will tend to move off the equator, so far as the reduction of the equatorial surface windspeed which result from such a shift lead to a high enough $\partial_\phi V$ which is able to offset $\partial_\phi h_{\mathrm{sfc}}$ such that Equation 3.1 maximizes off the equator. As $\eta$ becomes small, $\partial_\phi h_{\mathrm{sfc}}$ approaches zero over a larger part of the equatorial belt, making it trivial to support an off equatorial maximum in $h_{\mathrm{PBL}}$, and hence a double ITCZ. Likewise, if the near equatorial gradient in $\partial_\phi h_{\mathrm{sfc}}$ is large enough, the reduction of the surface winds that accompany a poleward shift in the convection will insufficiently reduce the equatorial $h_{\mathrm{PBL}}$, making it difficult to shift the maximum of $h_{\mathrm{PBL}}$ off the equator.

This line of reasoning is supported by experiments which break the coupling between the surface wind speed and the placement of the convection. For the case of a global constant near surface wind forcing of 5, 10 and 15 $\mathrm{ms}^{-1}$, so that $\delta V$ is by definition

zero, a single ITCZ (at the equator) emerges, irrespective of the convection scheme. Similar behavior was documented by Numaguti (1993). In the LS, N.std and T.std experiments the position of the ITCZ peak is coincident with large gradients in the near surface windspeed (Figure 3.2). These large gradients are not only a result of the ITCZ position but also a cause. For experiments in which the near surface windspeed input to the surface heat flux scheme is set to be piecewise constant with a value of $4\,\mathrm{ms}^{-1}$ near the equator, and to $10\,\mathrm{m\,s}^{-1}$ poleward of a certain latitude, an ITCZ forms at the position of the point wise discontinuity in the near surface windspeed, and shows little dependence on the choice of convective parameterization. In cases where the point wise discontinuity in the near surface winds is sufficiently poleward (locating at roughly 12 degrees of latitude) a third precipitation peak forms at the equator in addition to the double peaks close to the point where the near surface winds changed. If the point wise discontinuity is within about 2 degrees of the equator the two outer precipitation bands fuse into a single ITCZ.

These ideas, and the experiments that were conducted to test them, suggest that the primary control on the position of the ITCZ is the strength of the local SST gradient, but how large this gradient has to be can vary as a function of the convection scheme. Also the forcing at the upper boundary, namely the radiative cooling, has a controlling influence on the ITCZ position. Experiments in which ice cloud radiative effects are disabled show a significant shift of the ITCZ in poleward direction. Irrespective of how the latitudinal driving of convection is allowed to vary, it is clear that different convection schemes can couple differently to this driving. For the case of a system forced at the surface in different ways, a particular issue arises in terms of how a convection scheme couples to the large scale circulation in a way that determines the surface winds, and hence the distribution of boundary layer moist static energy.

## 3.2 The ITCZ position decoupled

The strong coupling between the convection scheme and the large scale circulation makes it difficult to simply compare experiments with different convection schemes. Small differences in the convection schemes can swing the balance of the feedback loop in ways that end up leading to large differences in where the convection locates, as well as in the large scale circulation in which it is embedded. Hence to study the effect of choices one makes in formulating the convection it is helpful to break the feedback loop that couples the convective position to the large scale dynamics. The previous discussion suggests that this should be possible by changing the wind dependence of the surface evaporation. We do so by prescribing the windspeed that is input to the scheme used to calculate surface heat exchange with the atmosphere. By prescribing these winds from a fixed climatology, it is possible to control the convective organization.

To illustrate this point, simulations were performed with the Nordeng convective parameterization in which the surface wind is taken from the climatology of simulations using the Tiedtke parameterization. Figure 3.4 shows the results from both wind forcings. The precipitation patterns are very similar under the same wind forcing, with only a hint that the Tiedtke parameterization favors a more poleward placement of the ITCZ. The single ITCZ under the Nordeng wind forcing has a little higher maximum and is slightly more peaked under the Nordeng parameterization (N.wndN) compared to the Tiedtke one (T.wndN). Similarly for Tiedtke wind forcing, the double ITCZ peak has a slightly higher maximum as well as the local minimum at the equator is more pronounced in the simulation with the Tiedtke parameterization (T.wndT) as compared to the simulation with the Nordeng parameterization (N.wndT). Differences between the N.std and the N.wndN as well as between T.std and the T.wndT are small, suggesting that zonal and temporal variations in the near surface wind couple weakly to the mean circulation.

These experiments suggest that by analyzing the subtle differences between simulations with the Tiedtke and Nordeng convection schemes under an identical wind forcing, it should be possible to understand how the details of each scheme affect its coupling to the large scale circulation. To do so requires an understanding of how the schemes behave differently under the same wind forcing. This is then the purpose of the following section.

It would also be possible to break the feedback loop at another place by prescribing the dry static energy and humidity of the free troposphere as seen by the convection scheme. This leads to similar results as compared to the wind forcing experiments.

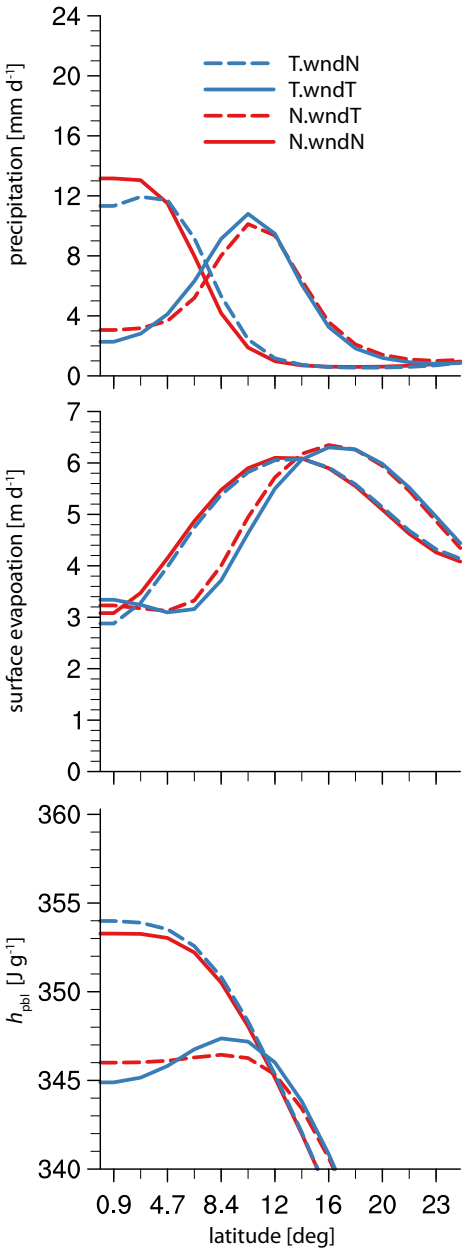


Figure 3.4: Time and zonal average precipitation, surface level horizontal wind and moist static energy in the planetary boundary layer for the experiments T.wndN, T.wndT, N.wndT and N.wndN.

# Chapter 4

# Convective Scheme Signatures for Fixed Wind Forcing

With the wind forcing fixed, the Tiedtke and Nordeng convective parameterizations produce similar latitudinal distributions of precipitation, $h_{\mathrm{PBL}}$ and surface evaporation (Figure 3.4), but rather different latitudinal distributions of convective available potential energy. This is evident in Figure 4.1, which shows difference between the moist static energy in the planetary boundary layer and the saturated moist static energy on the 500 hPa isobar. This difference is proportional to the adiabatic CAPE. Larger values imply greater instability, and as expected the instability is largest around the

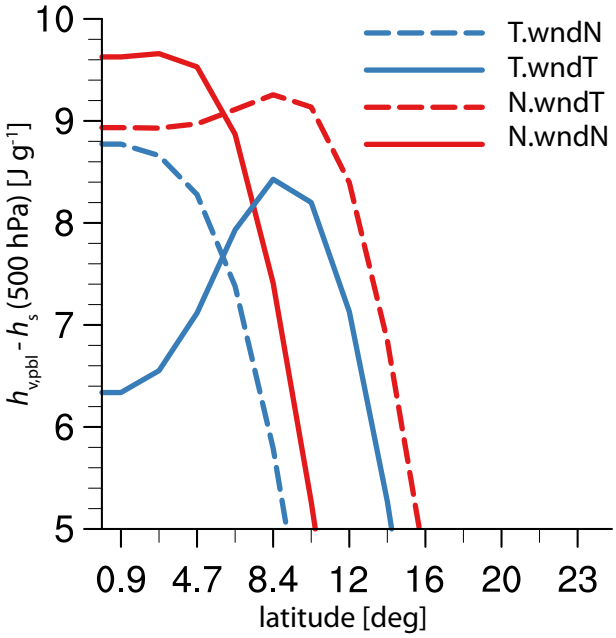


Figure 4.1: Boundary layer instability as measured by the difference between the moist static energy in the planetary boundary layer and the saturated moist static energy on the 500 hPa isobar for the experiments T.wndN, T.wndT, N.wndT and N.wndN.

position of the ITCZ precipitation maximum. The T.wndT simulation shows a strong decrease of instability (increased stability) from the precipitation maximum towards the equator. This enhanced stabilization toward the equator in the case of a double ITCZ is less pronounced in the N.wndT experiments. The tendency of Nordeng to have a flatter distribution of $h_{\mathrm{PBL}}$ is also evident in the simulations with the Nordeng wind forcing. Because gravity waves are effective in homogenizing temperature differences in the tropical free troposphere, these differences can be attributed to differences in $h_{\mathrm{PBL}}$. Indeed, Figure 3.4 indicates that $h_{\mathrm{PBL}}$ is relatively constant equatorward of its maximum value for the case of the Nordeng simulations (N.wndT), but drops by 2 J $\mathrm{g}^{-1}$ for the T.wndT case. In addition to the different latitudinal variations, the simulations with the Nordeng scheme are more unstable than the simulations using the Tiedtke scheme with the same wind forcing, even though the Tiedtke parameterization convects with a slightly larger maximum $h_{\mathrm{PBL}}$, e.g., Figure 3.4. Given that Tiedtke and Nordeng have the same moist static energy at cloud base this suggest that the deep convecting updrafts from Nordeng have larger lapse rates than Tiedtke.

Even with similar wind forcing and similar precipitation rates overall, the two schemes precipitate in a qualitatively different way. This is evident in Figure 4.2 which presents histograms of the convective precipitation rate for clouds located equatorward of 14°,

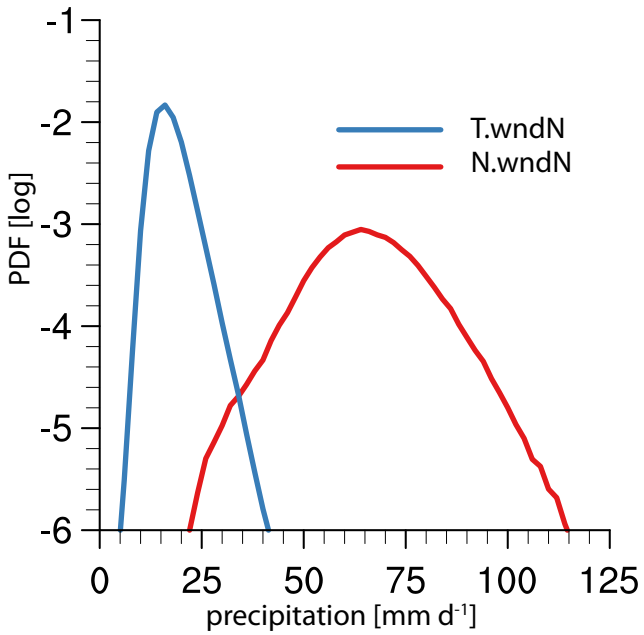


Figure 4.2: Precipitation flux histogram for single deep convecting events with a cloud top higher than 20 levels above the surface (roughly 250 hPa) for the experiments T.wndN and N.wndN from gridpoints located between 14 degree and the equator.

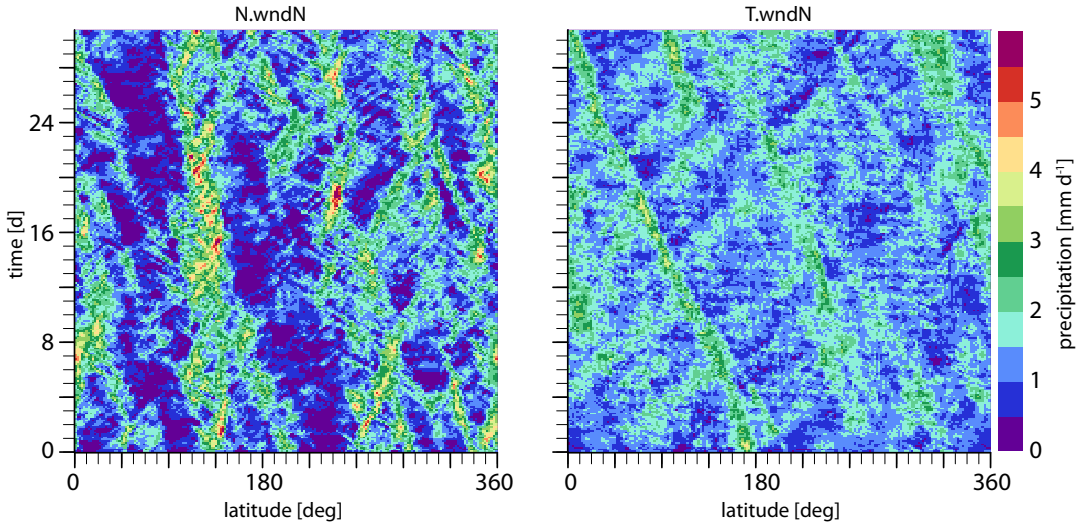


Figure 4.3: Hovmöller diagrams of the precipitation averaged over the tropical belt ($|\phi| \leq 10°$) for the experiments N.wndN and T.wndN.

whose tops reach above level 20 (corresponding to roughly 250 hPa). The Nordeng parameterization precipitates less often, but more intensely. These differences are also evident in Hovmöller diagrams of the precipitation averaged over the deep tropics ($|\phi| \leq 10°$), in Figure 4.3. Both parameterization show a rich spectrum of eastward and westward moving waves, but the precipitation is more homogeneously distributed across the equatorial belt in the experiments with the Tiedtke parameterization. The Nordeng parameterization tends to concentrate the deep convective activity into larger clusters, and allows for extended regions in which deep convection is strongly suppressed. These differences are associated with a different sensitivity of the two convection schemes to the free tropospheric humidity. This is illustrated by comparing how the precipitation covaries with column relative humidity, e.g., Figure 4.4, which is constructed following Bretherton et al. (2004). On average, Nordeng begins precipitating only at larger values of column relative humidity, which suggests that it couples more tightly to the distribution of free tropospheric humidity than does Tiedtke.

Because the saturation specific humidity depends on temperature non linearly, the column relative humidity weights lower levels, more strongly than higher levels especially the sub cloud layer. In our model at least, the sub cloud layer relative humidity has no direct influence on the updraft temperature, since there is no mixing at these levels. Although it is thought that variations in column relative humidity track those in the lower (between 850 and 550 hPa) troposphere, which have been shown to correlate more strongly with convective events (Neelin et al. 2009; Holloway and Neelin

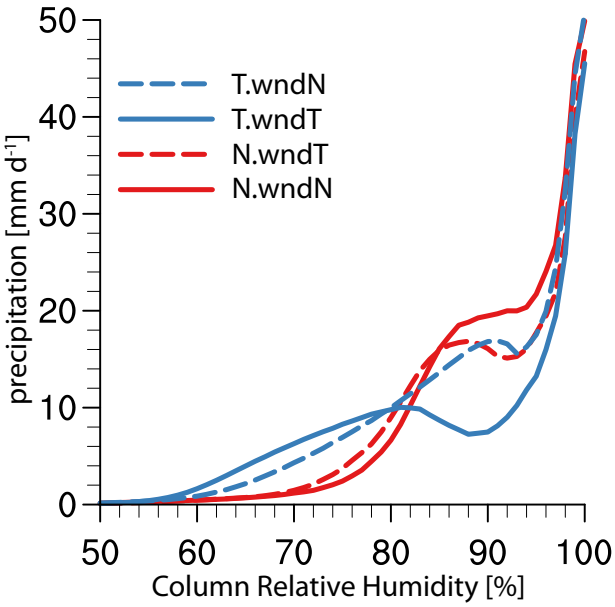


Figure 4.4: The average precipitation rate for column relative humidity histogram bins for the experiments T.wndN, T.wndT, N.wndT and N.wndN.

2009; Nuijens et al. 2009), it makes sense to look at variability in these layers directly. Figure 4.5 presents humidity histograms by height, where height is taken at model half levels as seen by the convective parameterization. Results for the N.wndT and T.wndT simulations are presented at three latitudes; the latitude where precipitation maximizes (10.3 degrees), one latitude equatorward of this point, and at a third latitude poleward of the precipitation maximums. The humidity histograms reveal a fundamentally different humidity height distribution for the two simulations. The main differences are concentrated in two layers. First in the levels 9 to 12 (about 700 to 550 hPa), which will be called the lower middle troposphere henceforth, and second above the lower middle troposphere between about 550 hPa and the tropopause, near 150 hPa. The lower middle troposphere sits between the level where shallow convection usually terminates and the melting level. This level has been identified as a preferred level of cumulus detrainment in the observational record (Johnson et al. 1999). The Nordeng simulations are significantly moister in the lower middle troposphere at all latitudes. At $\phi = 4.6°$ the lower middle troposphere average humidity is 61.1 % for N.wndT as compared to 46.7 % for T.wndT. Simulations with Tiedtke are almost 15 % drier there. Differences are less pronounced in the poleward direction, but still more than 5 % at 14°. In the layer between about 550 hPa and 150 hPa the Nordeng simulations show a pronounced bimodal humidity distribution. This distribution is characterized by one

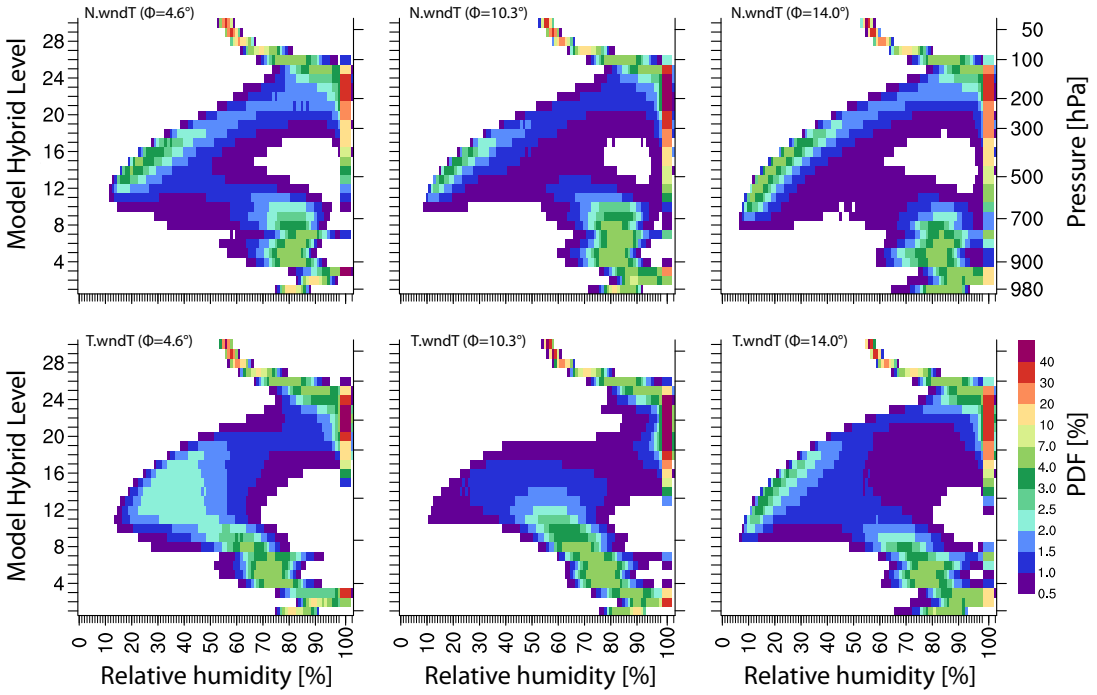


Figure 4.5: Humidity histogram by height depending on model hybrid levels for the latitudes equatorward, at, and poleward of the precipitation maximum for the T.wndT, N.wndT. experiments.

very dry regime with relative humidities down to 10 %, and which can be associated with continuous downdrafts in regions where deep convection is presumably not active, and one very moist regime with relative humidities around 100 %, which likely contains the convecting parts of the atmosphere. This bimodal humidity distribution also exists in the Tiedtke simulations but is much less pronounced, particular at the latitude where convection maximizes.

Summarizing, even for the situation in which the large scale conditions near the surface are fixed, and hence the latitude at which precipitation maximizes is the same for both parameterizations, with the Nordeng parameterization deep convection is more intermittent (Figure 4.3), and requires larger free tropospheric humidities to form. The high humidity sensitivity leads to a self amplification of humidity perturbations which allow dry regions to develop, even at latitudes where convection and precipitation maximizes (Figure 4.3). In addition, the Nordeng deep convection often terminates its updraft in the lower middle troposphere if it is to dry there, such in that case it acts as a form of cumulus congestus, which works to equilibrate the moisture in the lower middle troposphere to the boundary layer and increase the value of $h_{\mathrm{ft}}$ in the region

where it typically takes on its minimum value.

# Chapter 5

# Mechanisms Controlling Convective Organization

This section builds upon the results of the previous sections to develop and test a hypothesis as to why the Nordeng scheme tends to locate the ITCZ equatorward of the latitude favored by the Tiedtke scheme.

## 5.1 A Humidity Entrainment Feedback

Chapter 3 argued that the position of the ITCZ is determined by the manner in which convection couples to the large scale circulation. The articulation of this loop focused primarily on factors controlling $h_{\mathrm{PBL}}$ and the location of its maximum. To understand the differences between Tiedtke and Nordeng it proves useful to first ask how the two schemes would behave if $h_{\mathrm{PBL}}$ and $s_{\mathrm{ft}}$ (the free tropospheric dry static energy) would be horizontally homogeneous in the tropical region, but the free tropospheric humidity varied such that it tended to be more humid in the lower middle troposphere near the equator. To a first approximation Tiedtke's updraft model is non mixing and so it would see little impact of this humidity gradient, and would be coupled to the large scale circulation following the arguments of Chapter 3. For a strongly mixing updraft however, convection would be favored on the equatorial flank of the ITCZ, as updrafts will remain warmer and reach deeper in the more moisture rich air on the equatorward size of the ITCZ.

The idea that the Nordeng scheme convects less successfully in dry air, because it has a more mixing updraft, can be explored by comparing the convective success rate to the humidity histogram in the lower middle troposphere. This is illustrated with the help of Figure 5.1, in which the success rate is defined as the fraction of convective events that succeed in being deep (as defined by a cloud top higher than level 20, roughly 250 hPa) after deep convection was initially triggered. The figure shows the marked sensitivity of deep convection to the humidity in the lower mid troposphere for the Nordeng scheme as compared to the Tiedtke scheme. For Nordeng the success rate of deep convection is overall much lower than Tiedtke and falls to below 50 %

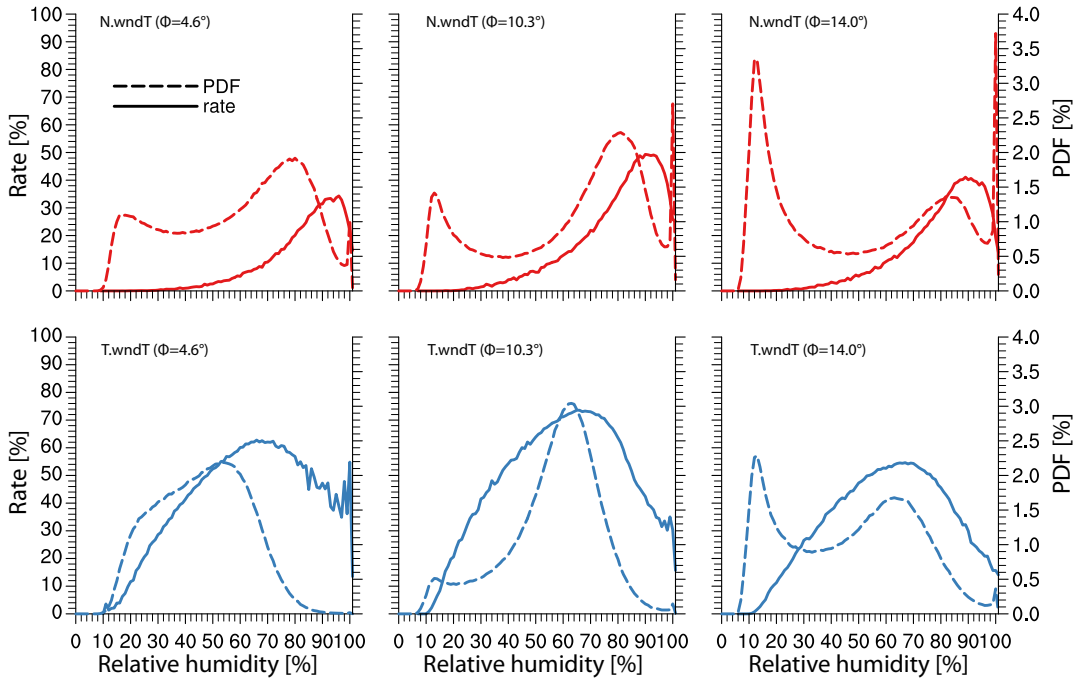


Figure 5.1: Histogram of average level 9-12 humidity (dashed) and convective success rate (solid) equatorward, at, and poleward of the precipitation maximum for the T.wndT, N.wndT. experiments. The latitudes and experiments are identical to those plotted in Figure 4.5. Convective success rate is defined as the ratio between the number of deep convecting events with a cloud top higher than 20 levels above the surface (approximately 250 hPa) and all events where the deep convective parameterization was initially triggered.

of its peak value at humidities below about 75 % in the lower middle troposphere. Whether or not convection becomes deep when using the Tiedtke scheme is however relatively independent of humidity, as humidities must fall below 30 % in the lower middle troposphere before the deep convective success rate falls to half of its peak value. Even then, Tiedtke is as successful at producing deep convection as Nordeng is in the best of circumstances. When this is combined with the tendency of both convective schemes, but particularly for Nordeng, atmospheres develop with more arid poleward flanks of the ITCZ. This clearly suggests that all things being equal the humidity gradients in the free troposphere will favor more equatorward convection in simulations using Nordeng, or for that matter any scheme whose updraft model mixes more strongly than Tiedtke (see Oueslati and Bellon 2012).

## 5.2 Testing the Effect of Humidity Coupling on the ITCZ Placement

To test the ideas developed above additional simulations were performed as described in Chapter 2.2 and Table 2.2. To test the effect of tropospheric humidity experiments were performed with both schemes in which the updraft model only saw relative humilities of 100 %. The results with the Tiedtke scheme with this change are practically indistinguishable from the standard Tiedtke simulations, which confirms that the Tiedtke scheme has a low sensitivity to humidity. With the 100 % forcing, the Nordeng scheme differs markedly from the standard Nordeng simulations, and develops a double ITCZ within one grid point of the corresponding Tiedtke experiment. This supports the argument that the humidity sensitivity can play a decisive role in how the convection couples to the large scale circulation. The complement of this experiment can be constructed by forcing a greater sensitivity to humidity of the Tiedtke scheme. This is performed by replacing the "actual" with the adiabatic cloud top height for the calculation of $p_*$. Under this configuration the results from the modified Tiedtke and the standard Nordeng experiment are almost identical, and the result of the standard Nordeng experiment is largely unchanged. This imposed sensitivity of the Tiedtke scheme can also be obtained if the cloud top height is simply restricted in the final updraft calculation by the actual cloud top height of the first updraft calculation, as it is done in the Nordeng scheme.

Armed with these insights, it is useful to reconsider the LS experiments. Because a higher updraft entrainment will reduce the updraft humidity closer to that of the environment, the maximum humidity sensitivity is reached when the updraft and environmental humidity are one and the same. This is the case in the large scale (LS) experiment, in which the deep convection parameterization is turned off. In this experiment a strongly peaked single ITCZ develops, according to the ideas described above.

The influence of the closure were tested in simulations where the Nordeng scheme was combined with the Tiedtke cloud base mass flux calculation (N.Tcbm) and vice versa (T.Ncbm). T.Ncbm is very similar to T.std, while N.Tcbm shows a double ITCZ with a precipitation maximum located at 6 degree opposite to the single ITCZ of N.std. This result can be understood if taking into account that the updraft temperature in the Tiedkte scheme is insensitive to atmospheric humidity, as is the Nordeng CAPE closure together with the Tiedtke scheme. On the other hand, the updraft temperature in the Nordeng scheme is quite sensitive to atmospheric humidity, as is the Nordeng CAPE closure in the Nordeng scheme. Tiedtke closure is per definition insensitive to the free troposphere. Thus, if the CAPE closure, in the Nordeng scheme is replaced with the moisture convergence closure the humidity sensitivity of the Nordeng scheme is reduced, which explains the resulting poleward shift of the ITCZ.

The trigger which decides between deep and shallow mode of the convection scheme has only a minor influence on the ITCZ placement (Equation 2.19).

## 5.3 Further Effects of Free Tropospheric Humidity

The free tropospheric humidity not only helps limit convection through its interaction with the updraft model, but also through its influence on $h_{\mathrm{ft}}$. A characteristic feature of the tropical atmosphere is the minimum in free tropospheric humidity near 700 hPa. This feature largely expresses the dryness of the lower free troposphere, and following Equation 3.1 also influences the equilibrium value of $h_{\mathrm{PBL}}$. More frequent deep convection favors a dry lower middle troposphere because there are less events with shallow cloudtop heights which moisten the lower middle troposphere. There is also evidence of a stronger meridional overturning in the case of more frequent deep convection. Both points are evident in Figure 4.5 wherein the dry downdraft branch of the circulation is more evident at latitudes away from the precipitation maximum, and the lower middle troposphere is everywhere drier, in the simulations with the Tiedtke parameterization. The tendency for weaker, more frequent, deep convection to more efficiently dry the lower troposphere reduces $h_{\mathrm{ft}}$ which following Equation 3.1 will lower $h_{\mathrm{PBL}}$ in less convective regions, as for instance is evident in the tendency for the Tiedtke simulations to show a more pronounced decrease in $h_{\mathrm{PBL}}$ equatorward of its maximum than is shown by simulations using the Nordeng parameterization, e.g., Figure 3.4.

# Chapter 6

# Influence of the vertical mixing profile on convection

## 6.1 Convection Scheme Setup

Chapter 5.1 presented a feedback loop mechanism which lead to the conclusion that the different ITCZ positions of the Tiedtke and Nordeng scheme with the Qobs sea surface temperature profile result from the stronger mixing of the convective updraft in the Nordeng scheme compared to the Tiedtke scheme. Therefore an increase (decrease) of the mixing rates in Tiedtke or Nordeng like convection schemes should shift the ITCZ in equatorward (poleward) direction. Unfortunately experiments with either the Nordeng or Tiedtke convection scheme have the disadvantage that even though the turbulent mixing constant can be prescribed, the organized entrainment and detrainment as well as the calculation of $p_*$ (see Equation 2.3) makes it difficult to either determine or prescribe the actual updraft mixing rates. Hence a precise analysis of the influence of updraft mixing on the ITCZ position is complex with those convection schemes. Further, with the Nordeng scheme's CAPE closure the cloudbase massflux depends on the mixing rates. Thus there is a second mechanism in which the mixing rates influence the convective organization. To circumvent these problems an idealized version of the Tiedtke scheme is used to study the influence of entrainment on the ITCZ position. This is called the "ideal Tiedtke" scheme henceforth. The ideal Tiedtke scheme does not distinguish between deep and shallow convection. Further the mixing process is separated into two independent parts; one which controls the influence of mixing on the intensive quantities of the updraft and one which controls the updraft massflux profile. The intensive quantities of the updraft are calculated using the same method as the turbulent mixing of the original Tiedtke scheme shallow convection, where both $\epsilon$ and $\delta$ are equal to a prescribed model-level dependent, mixing constant, $\mu$(level). The updraft massflux is calculated as:

$$\frac{\partial M_{\mathrm{up}}}{\partial z} = \begin{cases} +\epsilon M_{\mathrm{up}} & p > \frac{1}{2}(p_{\mathrm{cb}} + p_{\mathrm{ct}}) \\ -\delta M_{\mathrm{up}} & p \leq \frac{1}{2}(p_{\mathrm{cb}} + p_{\mathrm{ct}}) \end{cases} \tag{6.1}$$

with $\epsilon$ $=1.5 \cdot 10^{-4}\, m^{-1}$ and $\delta$ $=1.0 \cdot 10^{-4}\, m^{-1}$. This formulation leads to massflux profiles comparable to those observed with the original Tiedtke scheme. The cloudbase massflux is calculated identical to the original Tiedtke scheme. The ideal Tiedtke convection scheme presented above will be used for all experiments in this section because it makes it possible to directly prescribe the updraft mixing profile which allows to directly study the influence of the updraft mixing rate profile on the ITCZ position.

| Experiment | Mixing constant |
|---|---|
| M1 | $\mu = 1.5 \cdot 10^{-4}\, m^{-1}$ for all levels |
| M2 | $\mu = 2.0 \cdot 10^{-4}\, m^{-1}$ for all levels |
| M3 | $\mu = 2.5 \cdot 10^{-4}\, m^{-1}$ for all levels |
| M4 | $\mu = 3.0 \cdot 10^{-4}\, m^{-1}$ for all levels |
| M1-low | $\mu = 1.5 \cdot 10^{-4}\, m^{-1}$ below about 550 hPa and $\mu = 0$ above |
| M2-low | $\mu = 2.0 \cdot 10^{-4}\, m^{-1}$ below about 550 hPa and $\mu = 0$ above |
| M3-low | $\mu = 2.5 \cdot 10^{-4}\, m^{-1}$ below about 550 hPa and $\mu = 0$ above |
| M4-low | $\mu = 3.0 \cdot 10^{-4}\, m^{-1}$ below about 550 hPa and $\mu = 0$ above |

Table 6.1: Basic experiments with the ideal Tiedtke scheme

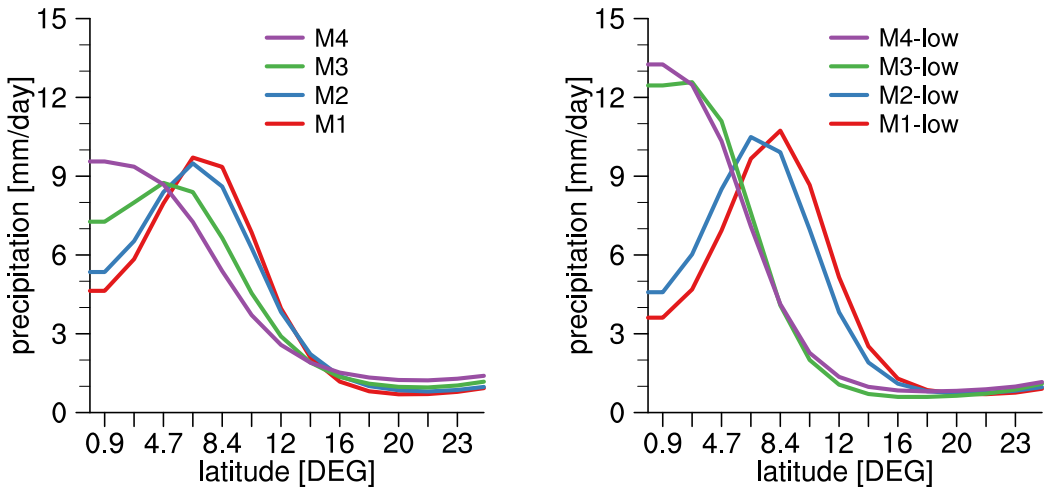


Figure 6.1: Time and zonal average precipitation for the various experiments with fixed mixing rate profiles from Table 6.1.

According to Chapter 5.1 the ITCZ should shift towards the equator if the mixing rates in the ideal Tiedtke scheme are increased. In order to verify this prediction two sets of experiments are performed with the ideal Tiedtke scheme; one where the mixing constant is set to one value for all model levels and another set where the mixing constant is set to one value for for the first 12 model levels from the surface, where level 12 corresponds to the mid troposphere and $p \sim 550\,\text{hPa}$ and zero above as listed in Table 6.1. The time and zonal average precipitation of these experiments (Table 6.1) is shown in Figure 6.1. In this figure a clear shift of the ITCZ towards the equator for increasing updraft mixing is evident as expected from the humidity entrainment effect on the feedback loop (Chapter 5.1).

If the main differences between the Tiedtke and Nordeng scheme are caused by a different strength of the updraft mixing as shown in Chapter 5.1 then the ideal Tiedtke scheme should also be able to reproduce either the results of T.std and N.std with a appropriate choice of the updraft mixing constant. Further this would also justify the use of the ideal Tiedtke scheme as a test bed to study the influence of the entrainment rates on the ITCZ position in either the Nordeng or Tiedtke scheme. Actually the time and zonal average precipitation from M1-low is quite close to that of the T.std experiment as well as the time and zonal average precipitation from M3-low is quite close to that of the N.std experiment. Also the humidity histograms of M1-low and M3-low (see Figure 6.2) show typical features of the T.std respectively N.std experiment eventhough there are some differences between T.std and M1-low, as can be seen comparing Figure 6.2 and Figure 6.2. Especially the M3-low experiment shows high probability in the 100% humidity histogram bin below 500 hPa like N.std while the M1-low experiment shows almost no probability there like T.std. Further at the ITCZ below 500 hPa the M3-low experiment shows the probability centered around 85% relative humidity like N.std while the average humidity is decreasing with height in the M1-low experiment like in the T.std experiment, especially at 0.933 degree. Therefore the results of the M1-low and the M3-low experiment support the analysis of Chapter 5.1 that the different results of the Nordeng and Tiedtke convection scheme mainly originate from their different average mixing rates rather than from other differences through the formulation of entrainment, detrainment or cloudbase massflux.

## 6.2 Mixing in the Upper Free Troposphere

Statistically the vast majority of convective events with the convection scheme in deep mode either terminate at or below model level 12 (about 550 hPa) and become shallow or they terminate above model level 20 (about 250 hPa) and become deep. Hence it is to be expected that convection is predominantly sensitive to the tropospheric humidity below 550 hPa while convection should show weak or no sensitivity to humidity above 550 hPa. Therefore the ITCZ positions should be approximately similar between the M$n$

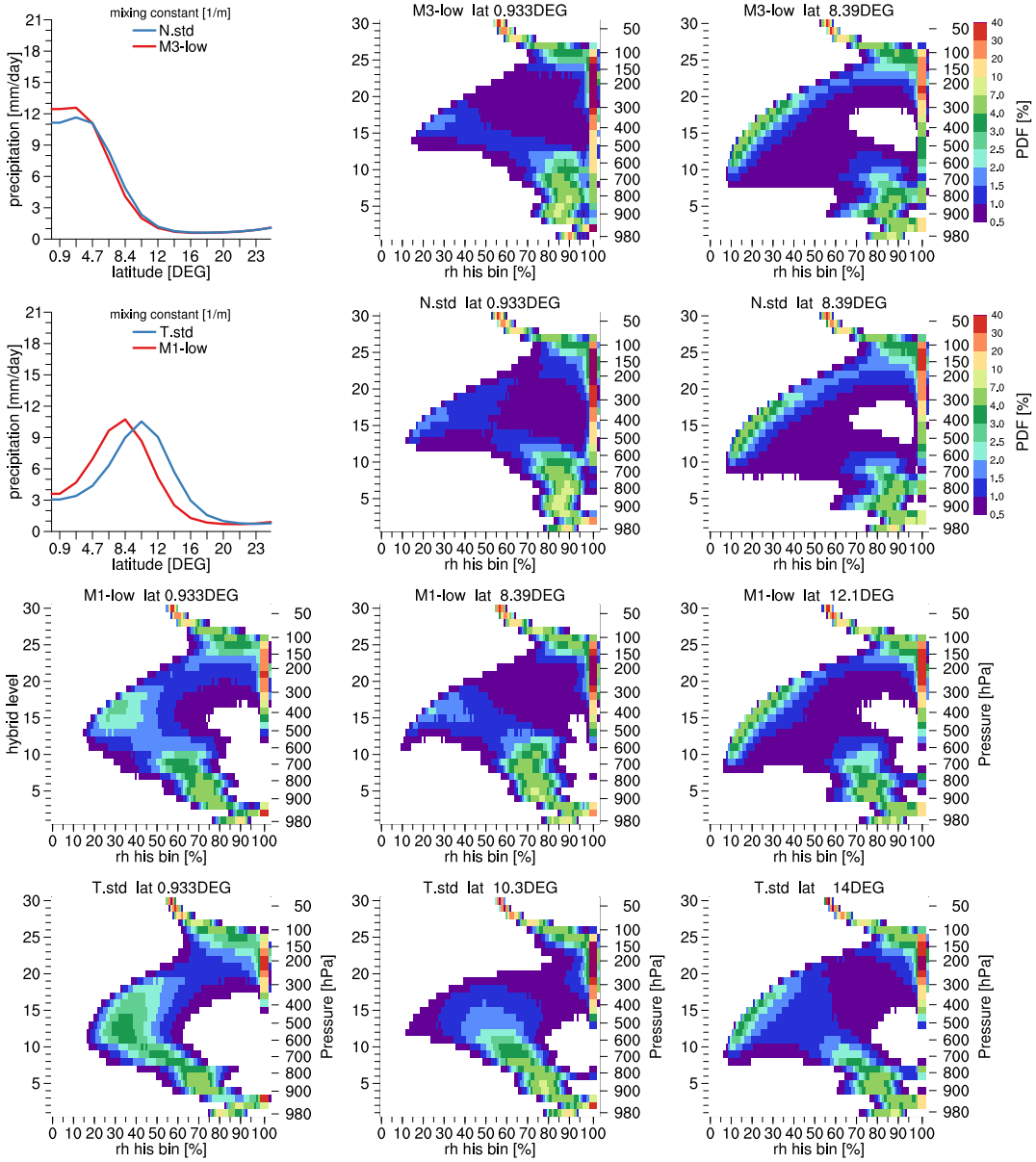


Figure 6.2: Time and zonal average precipitation for the M1-low, M3-low, N.std and T.std experiment as well as humidity histograms by height depending on model hybrid levels for two, respectively three latitudes for both experiments.

and the M$n$-low experiments since they only differ in their mixing rates above 550 hPa. Actually the ITCZ positions of M1 and M1-low as well as M2 and M2-low are quite

similar, while the ITCZ is even a bit closer to the equator in M3-low (M4-low) compared to M3 (M4). Further M3-low and M4-low show significantly higher precipitation rates compared to M3 and M4. This can be understood by taking into account that less mixing makes convection more efficient by transforming more condensate of the updraft into precipitation instead of detraining it. Even though this can not fully explain the different ITCZ pattern between the M$n$ and the M$n$-low experiments, these experiments suggest that the mixing in the upper part of the troposphere ($p \lesssim 550\,\mathrm{hPa}$) is of minor importance for ITCZ position unlike the mixing in the lower part of the troposphere ($p \gtrsim 550\,\mathrm{hPa}$).

## 6.3 Mixing in the Lower Free Troposphere

The last section demonstrated that mixing above approximately 550 hPa has almost no influence on the ITCZ position unlike mixing below 550 hPa. Nevertheless the variability of humidity is strongly height dependent as can be seen for example in Figure 6.2. The variability of humidity is especially high between roughly 700 hPa and 550 hPa where the humidity histogram splits into a dry and a moist regime where one part of the events have humidities around 10% while the other part of the events have

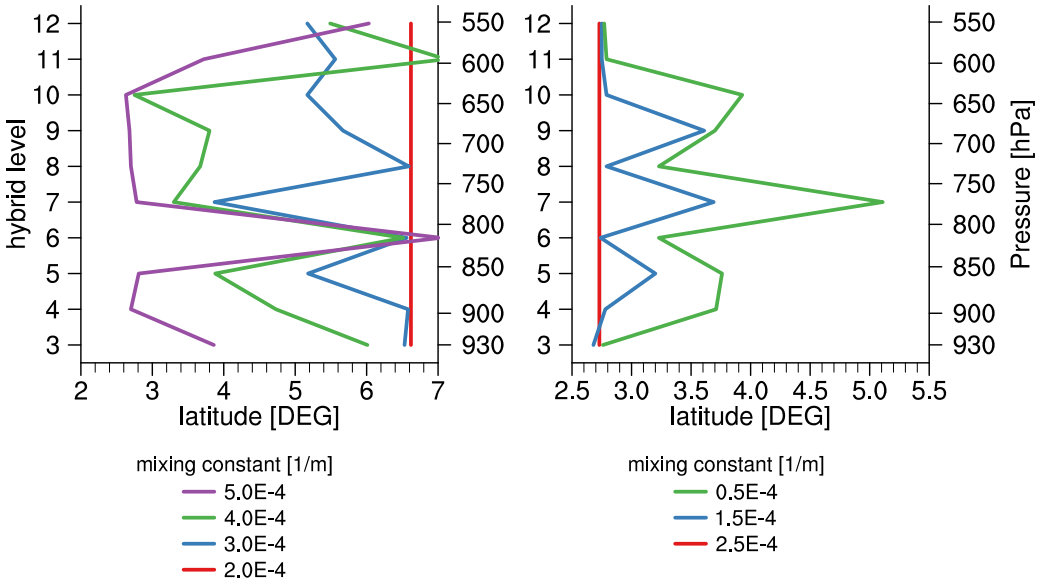


Figure 6.3: Left plot shows the ITCZ position for the M2-low experiment (red line) as well as M2-low based experiments where the mixing is increased to the value as indicated by the legend and the model level as indicated by the "hybrid level" axis. Right plot shows the same as the left but for the M3-low based experiments.

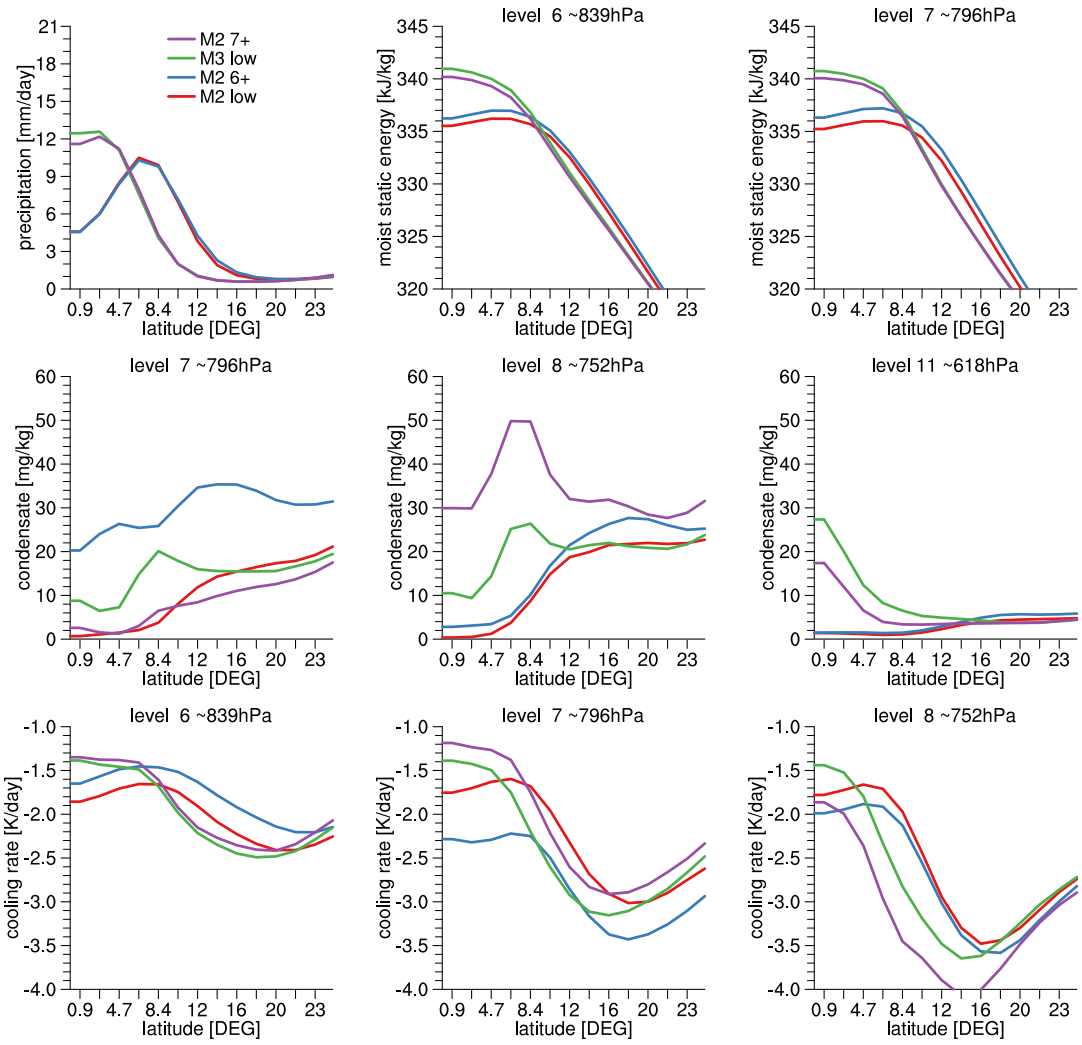


Figure 6.4: Time and zonal average precipitation for the experiments as indicted by the legend as well as moist static energy, specific liquid water plus ice mixing ratio and longwave radiative cooling rates for various hybrid levels.

humidities above 70%. Hence one could hypothesize that mixing above 700 hPa has a stronger influence on the ITCZ position than mixing below 700 hPa. To evaluate the influence of the vertical distribution of mixing on the ITCZ position two sets of experiments are performed. One is based on the M2-low experiment where the ITCZ located at 6.6 degree. Here the mixing constant is increased at a single model level from $2.0 \cdot 10^{-4}\, m^{-1}$ to either $3.0 \cdot 10^{-4}\, m^{-1}$, $4.0 \cdot 10^{-4}\, m^{-1}$ or $5.0 \cdot 10^{-4}\, m^{-1}$ to measure the

sensitive of the ITCZ position to an increase of mixing at a certain level. The ITCZ positions of these experiments are shown in Figure 6.3 in the left plot. The other set of experiments is based on the M3-low experiment where the ITCZ located at 2.7 degree. Here the mixing constant is decreased at a single model level from $2.5 \cdot 10^{-4}\, m^{-1}$ to either $1.5 \cdot 10^{-4}\, m^{-1}$ or $0.5 \cdot 10^{-4}\, m^{-1}$ to measure the sensitive of the ITCZ position to an decrease of mixing at a certain level. The ITCZ positions of these experiments are shown in Figure 6.3 on the right plot. The mixing rates in the first two model levels are not altered because they belong to the subcloud layer in which the updraft is non mixing.

Most of the experiments where the mixing parameter is increased show an equatorward shift of the ITCZ while most of experiments where the mixing parameter is decreased show an poleward shift of the ITCZ as expected from the humidity entrainment feedback. Opposite to the hypothesis mixing above 700 hPa does not have a stronger influence on the ITCZ position than mixing below 700 hPa. Nevertheless both sets of experiments show a quite distinct and complex dependence of the ITCZ position to the vertical distribution of mixing. One could argue that especially the increase of the mixing paramxeter from $2 \cdot 10^{-4}\, m^{-1}$ to $5 \cdot 10^{-4}\, m^{-1}$ in just one level leads to a unrealistic mixing profile. Nevertheless there is already a strong signal for the weakest forcing where the mixing parameter is only increased by 50%. Hence the distinct vertical dependence can not be a result of an unrealistic mixing profile. Instead there must be a physical explanation for it.

In order to identify the mechanism which caused the distinct vertical dependence two extreme opposite cases will be compared. First the M2-low based experiment in which the mixing is increased to $5 \cdot 10^{-4}\, m^{-1}$ in model level 7 (795 hPa), which shows a pronounced shift of the ITCZ towards the equator and will be called M2-7+ henceforth. Second the M2-low based experiment in which the mixing is increased to $5 \cdot 10^{-4}\, m^{-1}$ in model level 6 (840 hPa), which show even a small shift of the ITCZ in poleward direction and will be called M2-6+ henceforth. Results of those two experiments are shown in Figure 6.4. Further to better understand what happens when mixing is increased at one level, the experiments M2-low and M3-low will be used as a reference cases with a vertical homogeneous mixing profile below 550 hPa. Advantageously the precipitation rates of M2-low and M2-6+ as well as M3-low and M2-7+ are almost similar (Figure 6.4), which helps to identify what distinguishes the vertical homogeneous from the vertical inhomogeneous mixing experiments, since most physical quantities like the moist static energy profile are predominantly a function of the ITCZ position.

M2-low and M2-6+ as well as M3-low and M2-7+ mainly differ from each other in their longwave radiative cooling rates, distribution of water condensate and moist static energy. M2-6+ shows a higher moist static energy at level 6 (840 hPa) and 7 (795 hPa) compared to M2-low which counteracts the higher mixing of M2-6+ and prevents the updraft from loosing more moist static energy compared to M2-low, which explains

why in M2-6+ the ITCZ is not moving towards the equator compared to M2-low even though the mixing rates are higher. Opposite to that the moist static energy at level 6 (840 hPa) and 7 (795 hPa) is lower in M2-7+ compared to M3-low which makes the higher mixing of M2-7+ compared to M2-low even more efficient in decreasing the updraft moist static energy and pushes the ITCZ towards the equator as expected from the humidity entrainment feedback (see Chapter 5.1). The different moist static energies are most probably a result of the different longwave radiative cooling rates. While M2-6+ shows a weaker cooling rate at level 6 (840 hPa) and a stronger cooling rate at level 7 (795 hPa) and 8 (750 hPa) compared to M2-low, M2-7+ shows a lower cooling rate at level 7 (795 hPa) and a higher cooling rate at level 8 (750 hPa) compared to M3-low. The different longwave radiative cooling rates are most probably influenced by a different distribution of cloud liquid water. M2-6+ shows higher amount of liquid water at level 7 (795 hPa) compared to M2-low while M2-7+ shows lower amount of liquid water at level 7 (795 hPa) and a higher at level 8 (750 hPa) compared to M3-low.

The reason why the two extreme opposite cases, M2-6+ and M2-7+, are connected to model level 6 and 7 is most probably the fact that the levels 7 and 8 are the preferred termination level of the shallow convective clouds and thus host the highest amount of liquid water except for the cloud which sits on top of the boundary layer and therefore changes here should have the highest influence on the cloud radiative effect. Nevertheless the mechanism which connects the mixing with the distribution of cloud liquid water remains unclear. Further also the connection between moist static energy, radiative cooling and cloud liquid water profile needs to be verified by further research as well as the analysis should be expanded on all the other experiments in which the mixing rates are increased or decreased at on model level (Figure 6.3). It can be concluded that the experiments in this section showed a quite distinct and complex dependence of the ITCZ position to the vertical distribution of mixing below 550 hPa which can not fully be understood by the presented analysis and hence should be further explored.

## 6.4 Mechanisms of Lower Free Tropospheric Mixing

Figure 5.1 showed that for the Nordeng scheme deep convection is strongly suppressed if the average humidity between 550 hPa and 700 hPa is below about 70%. Therefore one could hypothesize that mixing of dry air has a stronger influence on the humidity entrainment feedback and thus on the ITCZ position as mixing of moist air. Hence, if a mixing rate which depends on the relative humidity is used one would expect that in order to get same ITCZ position as in one of the M$n$ low experiments the mixing rates for that relative humidities which have the strongest influence on the ITCZ position should be similar as in the according M$n$ low experiment. Equation 6.2 shows a mixing rate $\mu$ which linearly depends on the environmental humidity RH, where $r$ and $\epsilon_0$ are

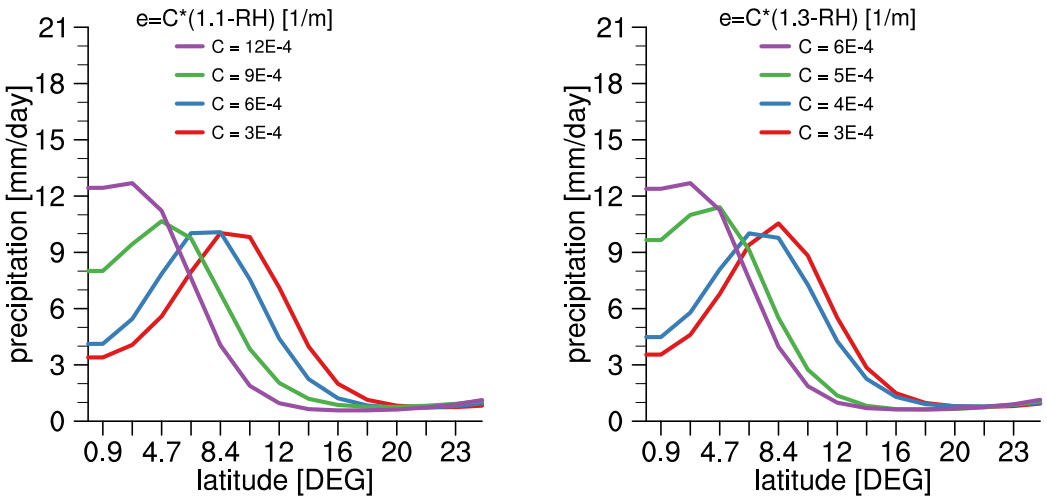


Figure 6.5: Time and zonal average precipitation for the experiments with relative humidity dependent mixing rates.

constants.

$$\mu = \epsilon_0 \big(r - \mathrm{RH}(z)\big) \tag{6.2}$$

This mixing rate formula is adaptation of Equation 22 from de Rooy et al. (2012) without the height dependent scale to have a better comparability to the other mixing rate experiments discussed here. Experiments are performed with $\epsilon_0 = 3$, 4, 5 or $6 \cdot 10^{-4}\, m^{-1}$ for r = 1.3 (Figure 6.5, right plot) and $\epsilon_0 = 3$, 6, 9 or $12 \cdot 10^{-4}\, m^{-1}$ for r = 1.1 (Figure 6.5, left plot). As expected from the humidity entrainment feedback the ITCZ shifts towards the equator for increasing values of $\epsilon_0$ for both r1.1 and r1.3. For the M$n$ low experiments a single ITCZ form for $\mu = 2.5 \cdot 10^{-4}\, m^{-1}$ (M3 low). For r1.1 a single ITCZ forms for $\epsilon_0 = 12 \cdot 10^{-4}\, m^{-1}$ such that $\mu = 2.5 \cdot 10^{-4}\, m^{-1}$ for RH = 89.2% and for r=1.3 a single ITCZ forms for $\epsilon_0 = 6 \cdot 10^{-4}\, m^{-1}$ such that $\mu = 2.5 \cdot 10^{-}4\, m^{-1}$ for RH = 88.3%. For similar ITCZ positions the mixing rates are much higher for relative humidities below about 70% in r1.1 and r1.3 compared to the M$n$ low experiments. Also for similar ITCZ positions the mixing rates for humidities below about 70% are much higher in the r1.1 compared to the r1.3 experiments. On the other hand for similar ITCZ positions the mixing rates in the about 75% to 100% humidity range are similar in either the r1.1, r1.3 and the M$n$ low experiments suggesting mixing with air with humidities between about 75% to 100% has the strongest influence on the ITCZ placement, which is an unexpected result according to the initial hypothesis of this section. Nevertheless Chapter 6.2 showed that mixing below 550 hPa dominates the ITCZ placement and Figure 6.2 shows that the majority of all events in the M3

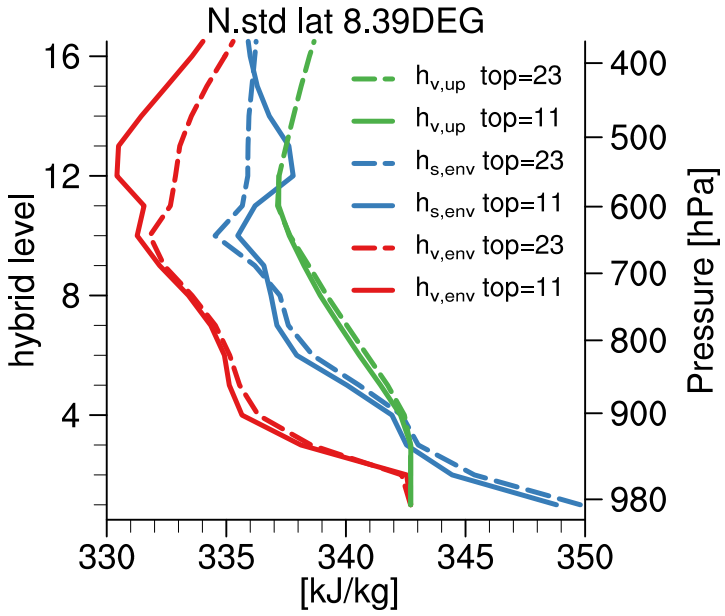


Figure 6.6: Shows the average environmental moist static energy ($h_{\mathrm{v,env}}$), environmental saturated moist static energy ($h_{\mathrm{s,env}}$) and the updraft moist static energy ($h_{\mathrm{v,up}}$) from the N.std experiment for either all deep events with a cloudtop at model level 11 or 23 at 8.39 degree latitude.

low experiment below 550 hPa have humidities between 75% to 100% except some very dry events between 700 hPa and 550 hPa. Hence it is to be assumed that mixing in the whole layer from cloudbase up to 550 hPa with air of 75% to 100% humidity influence the ITCZ position rather than mixing with very dry air located between 700 hPa and 550 hPa. Respectively the updrafts which encounter the dry regime terminate anyway independent of changes in the mixing rates, except if the mixing rates are strongly reduced under dry humidities like in the Tiedtke scheme.

Experiments have shown that triggering of deep convection plays only a minor role for the ITCZ placement. Therefore the ITCZ placement depends on suppressing deep convection outside the ITCZ region by terminating the updraft below about 550 hPa through the loss of buoyancy. The updraft looses its buoyancy if its moist static energy falls below the saturated moist static energy of the environment. Hence in order to understand why mixing with environmental air of humidities between about 75% to 100% dominates the ITCZ placement, a characteristic case shown by Figure 6.6 will be analyzed. Figure 6.6 shows time and zonal average profiles from the N.std experiment at 8.39 degree latitude for either all events where the convection scheme is in deep

mode and the cloudtop is located at level 11 (600 hPa) or 23 (170 hPa). These cloudtop heights are chosen because level 23 has the highest probability for a deep cloudtop and level 11 represents the deepest shallow cloudtop with a high probability. Events with cloudtop heights between level 12 (550 hPa) and 20 (250 hPa) are very rare. Further the latitude 8.39 degree is chosen because it is located at the flank of the ITCZ where still a high number off deep clouds are observed as well as a high number of shallow clouds. The profiles shown in Figure 6.6 are the environmental moist static energy ($h_{\mathrm{v,env}}$), environmental saturated moist static energy ($h_{\mathrm{s,env}}$) and the updraft moist static energy ($h_{\mathrm{v,up}}$). The difference between $h_{\mathrm{v,env}}$ and $h_{\mathrm{v,up}}$ is an indicator for how much moist static energy the updraft will lose by a certain amount of mixing, while the difference between $h_{\mathrm{s,env}}$ and $h_{\mathrm{v,up}}$ is an indicator for how much moist static energy the updraft can lose without loosing its buoyancy and terminating. Below model level 11 $h_{\mathrm{v,env}}$ and $h_{\mathrm{v,up}}$ are almost similar for both cloudtop cases and are almost decreasing linearly with height. Further the difference between $h_{\mathrm{v,env}}$ and $h_{\mathrm{v,up}}$ is almost constant with height which suggests a approximately height independent mixing efficiency between about model level 4 (900 hPa) to 10 (640 hPa). The temperature variation of the environment at model level 12 (550 hPa) finally terminates the shallow case while the deep case is still buoyant.

The M$n$ and the M$n$ low experiments showed that the ITCZ position mainly depends on the strength of mixing below 550 hPa through a prescribed vertically homogeneous mixing constant. This means that the ITCZ placement depends on the effect that with increasing mixing rates the updraft moist static energy lapse rate increases and thus for an increasing number of updrafts the updraft moist static energy falls below the saturated moist static energy of the environment below 550 hPa and therefore an increasing number updrafts terminate below 550 hPa. But for a small increase of the mixing rates to take effect a substantial number of updrafts must have a vertical moist static energy profile which exceeds the saturated moist static energy of the environment only slightly somewhere below 550 hPa. Thus a small increase in the updraft moist static energy lapse rate can lead to the loss of buoyancy below 550 hPa. Taking the high saturated moist static energy lapse rate of the environment between 900 hPa and 650 hPa (Figure 6.6) into account and not assuming unrealistically high mixing rates the only plausible solution which explains the mixing rate dependence of the ITCZ position is a continuously high mixing rate over the whole cloud layer below 550 hPa. Actually the case illustrated in Figure 6.6 shows a almost linear decrease of the updraft moist static energy with height between 900 hPa and 600 hPa. Further it should be taken into account that mixing with relative moist air below 550 hPa is efficient in draining moist static energy from the updraft. Since through the high saturated moist static energy lapse rate of the environment even mixing with saturated air would still be efficient in draining moist static energy from the updraft.

In summary the humidity entrainment effect and therefore ITCZ position depends

on a continuously high mixing rate throughout the whole layer between 900 hPa and 550 hPa such that the updraft moist static energy is reduced close to the saturated moist static energy profile of the environment which shows a distinct minimum around 650 hPa. Thus a small change of the mixing rates or a small variation in the environmental moist static energy can make the difference between a cloudtop height around 170 hPa or below 550 hPa. Herewith ITCZ placement mainly depends on mixing with air of humidities around 90% rather than on mixing with air of humidities below 70%. Nevertheless experiments show a quite distinct and complex dependence of the ITCZ position on the vertical distribution of mixing, while a final explanation for this dependence remains unclear.

# Chapter 7

# Influence of Radiative Cooling on Convective Organization

This chapter will analyze how the water vapor and cloud radiative effect is coupling on the feedback loop, discussed in Chapter 3.1 and 5.1, and thus have influence the ITCZ position.

Longwave radiative cooling destabilizes the troposphere above the subcloud layer, which is referred to as the free troposphere henceforth, and such increases the amount of energy available to convection. Nevertheless as discussed in section 3.1 gravity waves are efficient in homogenizing the thermal structure of the free troposphere within the tropics, thus a local increase in radiative cooling will not increase the amount of energy available to convection relative to other regions the tropics. Nevertheless radiative cooling, convective heating and the large scale vertical velocity are about balancing each other. Hence strong convective heating leads to large scale updrafts while with suppressed deep convection radiative cooling prevails and leads to large scale subsidence. Since the saturation water vapor pressure highly non linearly depends temperature there exist a steep vertical gradient in the specific water vapor mixing ratio of the free troposphere. Therefore the vertical profile of either the specific and relative humidity primarily depends on the vertical velocity. Hence in regions with strong convective heating the free troposphere is moist while it is dry elsewhere. Chapter 5.1 showed the importance of free tropospheric humidity for convective organization and the formation of a single ITCZ. Therefore it is important to understand how radiative cooling influences the free tropospheric humidity relative to the convective heating. If the radiative cooling is weaker in the ITCZ and stronger poleward of the ITCZ, it would amplify the effect of convective heating and thus increase the lateral humidity gradient between the ITCZ and the region poleward of it (on-off ITCZ humidity gradient) leading to a more equatorward position of the ITCZ and vice versa.

Chapter 6.2 showed that mixing below 550 hPa dominates the humidity entrainment effect (Chapter 5.1). Further the updraft is non entraining in the subcloud layer which is located below 900 hPa. Therefore further analysis will focus on the water vapor, liquid and ice radiative effects on the longwave radiative cooling rates in the layer

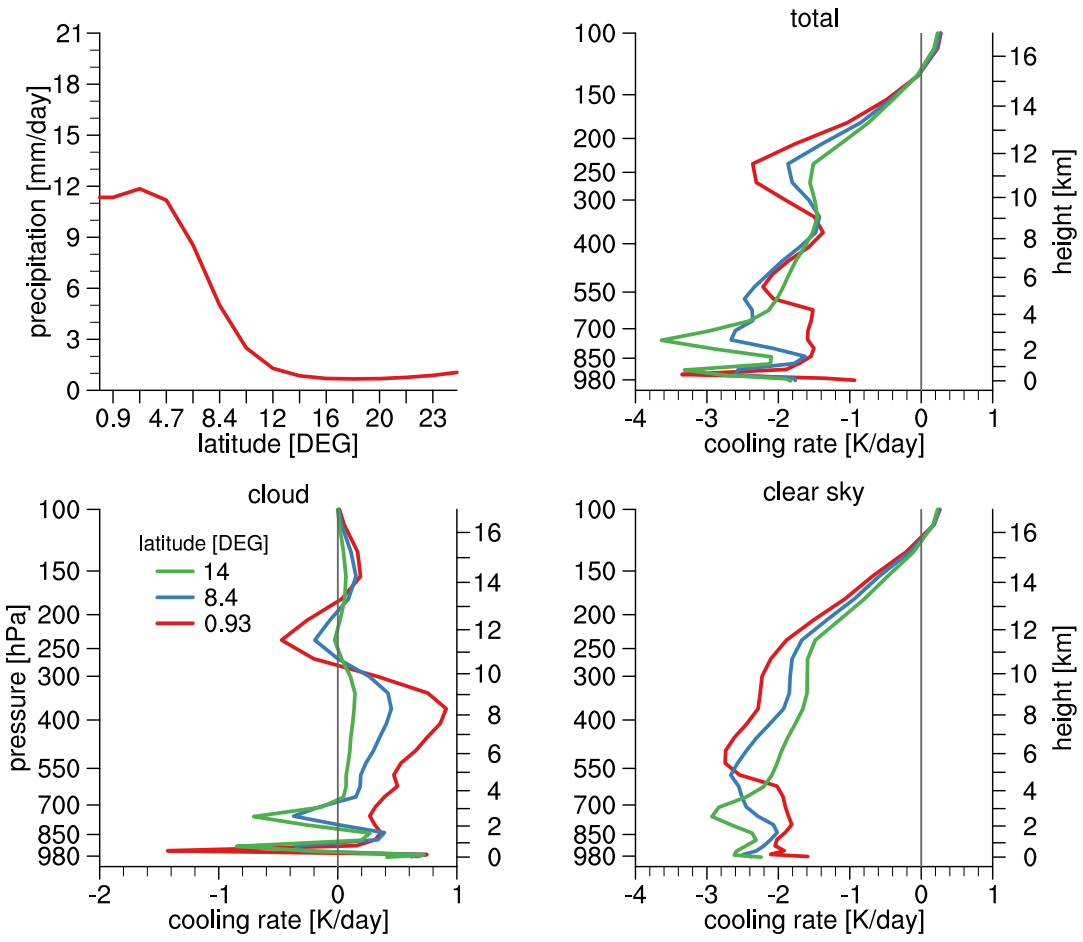


Figure 7.1: Time and zonal average precipitation and total, cloud and clear-sky longwave radiative cooling rates for the N.std experiment.

between 900 hPa and 550 hPa, just below the freezing level, which will be called the lower troposphere henceforth. Actually there is a distinct on-off ITCZ total cooling rate difference in the lower troposphere in the N.std experiment, as can be seen in the upper right plot of Figure 7.1. This on-off ITCZ cooling rate difference is either caused by the water vapor and cloud radiative effect, as can be seen in the lower two plots in Figure 7.1. The part of the total radiative cooling which depends on the water vapor radiative effect is represented by the clear sky radiative cooling rates and the part which depends on the cloud radiative effect is represented by the difference between the total and the clear sky radiative cooling rates. In the next two sections the influence of the water vapor and cloud radiative effect on the ITCZ position will be analyzed separately

from each other.

## 7.1 Water Vapor Radiative Effect

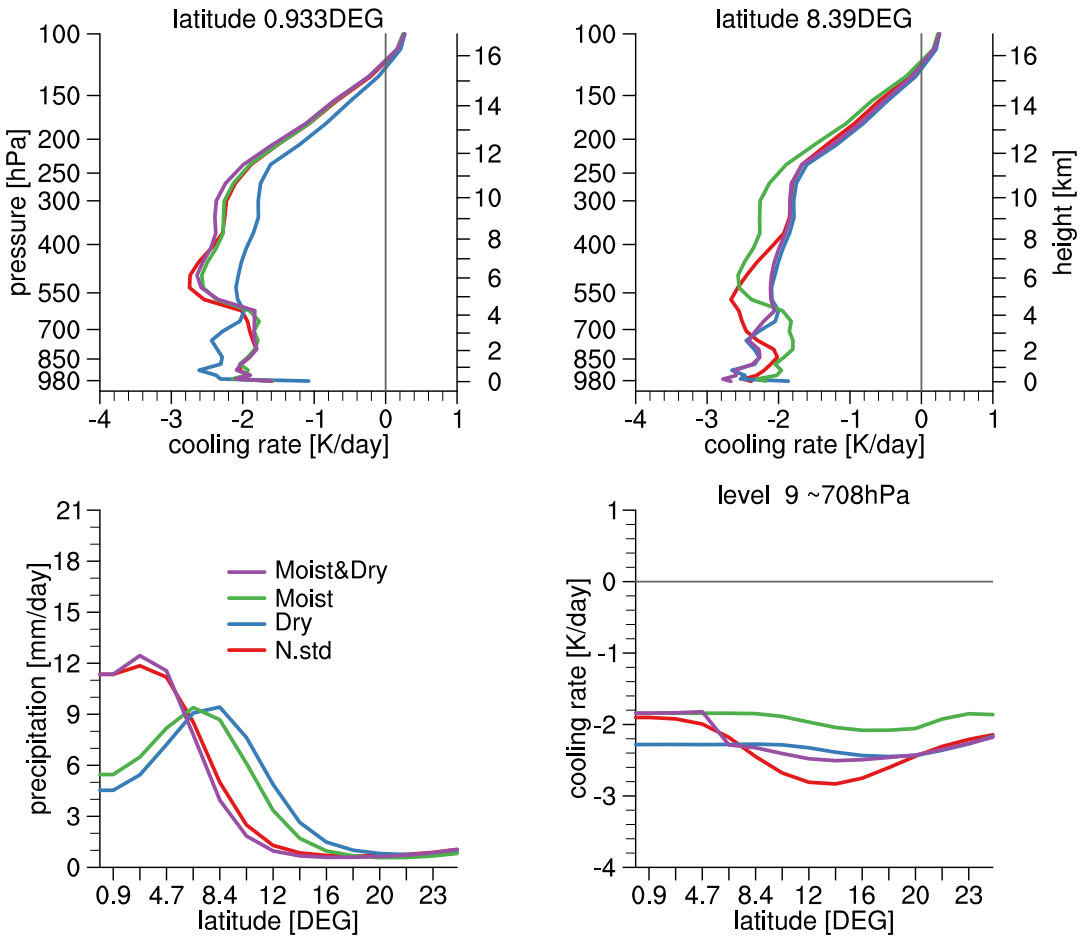


Figure 7.2: Time and zonal average precipitation and clear-sky longwave radiative cooling rates for the Moist&Dry, Moist, Dry and N.std experiments.

In order to analyze the influence of the water vapor radiative effect on the ITCZ position several experiments are performed with the configuration of the N.std experiment with modifications of the water vapor input to the radiative transfer scheme. The on-off ITCZ clear sky cooling rate difference in the lower troposphere is caused by the on-off ITCZ humidity difference which is characterized by a relatively moist free troposphere at the ITCZ and a dry free troposphere off the ITCZ. On the other hand the

on-off ITCZ clear sky cooling rate difference is also a cause of the on-off ITCZ humidity difference by its influence on the vertical velocity. Three experiments are performed where the water vapor input to the radiative transfer scheme 20 degree around the equator is fixed to a climatology using actual time and zonal averaged vertical profiles of the specific water vapor mixing ratio from the N.std experiment. For the "Moist" experiment the moist profile from the grid point at 1 degree at the center of the ITCZ in the N.std experiments is used. For the "Dry" experiment the dry profile from the grid point at 14 degree, where the vertically integrated longwave radiative cooling shows a maximum in the N.std experiments, is used. And for the Moist&Dry experiment the vertical profile from the grid point at 1 degree is used for the first three grid point from the equator and the vertical profile from the grid point at 14 degree is used for the remaining gridpoints until 20 degree off the equator. Figure 7.2 shows these three experiments along with the N.std experiment.

The Moist&Dry experiment shows the precipitation concentrated close to the equator very similar to the N.std experiment. While both the Moist and Dry experiment show a double ITCZ with a maximum around 8 degree. The clear sky cooling rates of the Moist and the Dry experiment are almost independent of latitude opposite to N.std as can be seen by the radiative cooling rate of model level 9 (Figure 7.2). This qualitative result is representative for the whole lower troposphere. Nevertheless the absolute cooling rates in the lower troposphere are much higher in the Dry compared to the Moist experiment. This result shows that the absolute amount of radiative cooling in the lower troposphere has almost no influence on the ITCZ position since it dose not influence the on-off ITCZ humidity difference. On the other hand the lack of a meridional radiative cooling rate difference strongly weakens the humidity entrainment feedback and leads to a large shift of the ITCZ off the equator. Hence the on-off ITCZ radiative cooling gradient through the on-off ITCZ humidity gradient in the lower troposphere is a crucial factor for the humidity entrainment feedback to push the ITCZ towards the equator. Even though the vertical and meridional distribution of the radiative cooling in the Moist&Dry compared to the N.std experiment diverge from each other, both experiments show almost the same ITCZ pattern emphasizing the importance of the absolute strength of the on-off ITCZ radiative cooling gradient over details in the vertical and meridional distribution of radiative cooling for the ITCZ pattern.

One could also argue that the increased cooling above 550 hPa at the center compared to the flank of the ITCZ (Figure 7.2) leads to an higher instability of the upper troposphere against deep convection at the center of the ITCZ. But the weak Coriolis force close to the equator gravity waves homogenize the thermal structure of the free troposphere very efficiently and thus keep the lateral instability gradient of the upper troposphere small. Therefore the influence of the increased cooling above 550 hPa on deep convection is small. This should be verified by inverting the Moist&Dry to a

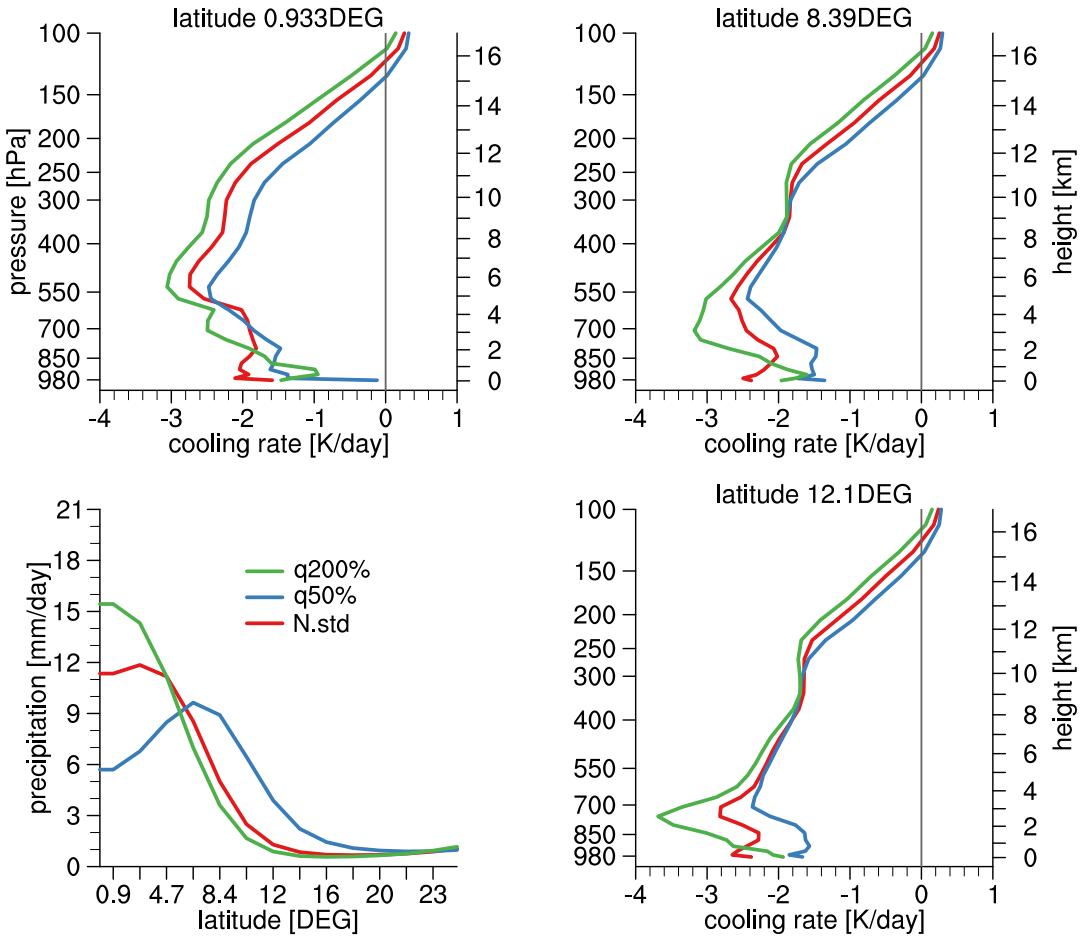


Figure 7.3: Time and zonal average precipitation and clear-sky longwave radiative cooling rates for the q200%, q50% and N.std experiments.

Dry&Moist experiment where the dry profile is used close to the equator and the moist profile elsewhere.

Instead of using a water vapor climatology one could also scale the input of water vapor mixing ratio to the radiative transfer scheme. Two experiments are performed where water vapor mixing ratio input to the radiative transfer scheme is multiplied by a factor of 2 (q200%), respectively 0.5 (q50%) within 20 degrees off the equator (Figure 7.3). The higher humidities of the q200% experiment lead to generaly higher cooling rates compared to the N.std experiment, while the lower humidities of the q50% experiment lead to generally lower cooling rates compared to the N.std experiment in the lower troposphere similar as with the Moist and Dry experiment. Even though the

different ITCZ positions made it difficult to compare the difference between off and on ITCZ cooling in the lower troposphere is more pronounced in q200% (0.93 vs. 8.93 degree) relative to N.std, while the difference is less pronounced for q50% (8.39 vs. 12.1 degree). Thus the resulting stronger peaked precipitation maximum of the q200% experiment compared to the N.std experiment and the shift of the precipitation peak off the equator in the q50% experiment compared to the N.std experiment fully fits the hypothesis that the strength of the on-off ITCZ cooling rate difference which amplify the vertical motion difference and thus the on-off ITCZ humidity difference is a crucial for the humidity entrainment feedback to push the ITCZ in equatorward direction.

In summary the on-off ITCZ convective heating difference leads to a on-off ITCZ humidity difference in the free troposphere. The on-off ITCZ humidity difference again enforces deep convection at the ITCZ and suppresses deep convection off the ITCZ enforcing the on-off ITCZ convective heating difference. Further the on-off ITCZ humidity difference leads to a on-off ITCZ radiative cooling difference in the 550 hPa to 900 hPa layer which again enforces the on-off ITCZ humidity difference and thus the on-off ITCZ convective heating difference. Thereby the self enforcing of the on-off ITCZ humidity difference by the influence of water vapor on the radiative cooling rates is an essential factor supporting the humidity entrainment feedback to push the ITCZ towards the equator.

## 7.2 Cloud Radiative Effect

| Name | Hybrid Levels | Pressure | typical cloud cover | typical mixing ratio |
|---|---|---|---|---|
| CL1 | 1 to 5 | 980 to 880 | 16% | 40 mg/kg |
| CL2 | 6 to 9 | 840 to 710 | 8% | 25 mg/kg |
| CL3 | 10 to 14 | 660 to 490 | 7% | 10 mg/kg |
| CL4 | 15 to 25 | 450 to 130 | 50% | 16 mg/kg |

Table 7.1: Definition of the four cloud types used for the cloud radiative experiments.

In the N.std experiment the clouds in the tropical region can be classified into four different characteristic types, which will be named CL1 to CL4 henceforth. Characteristic values of these cloud types are shown in Table 7.1. CL1 is the cloud which sits on top of the boundary layer all over the tropics at about 930 hPa and has a typical cloud cover of 16%. The CL2 cloud is mainly located poleward of the ITCZ and is located at the typical neutral buoyancy height of shallow convective clouds at about 770 hPa. CL2 has a typical cloud cover of 8%. The CL3 cloud is located at the ITCZ just below

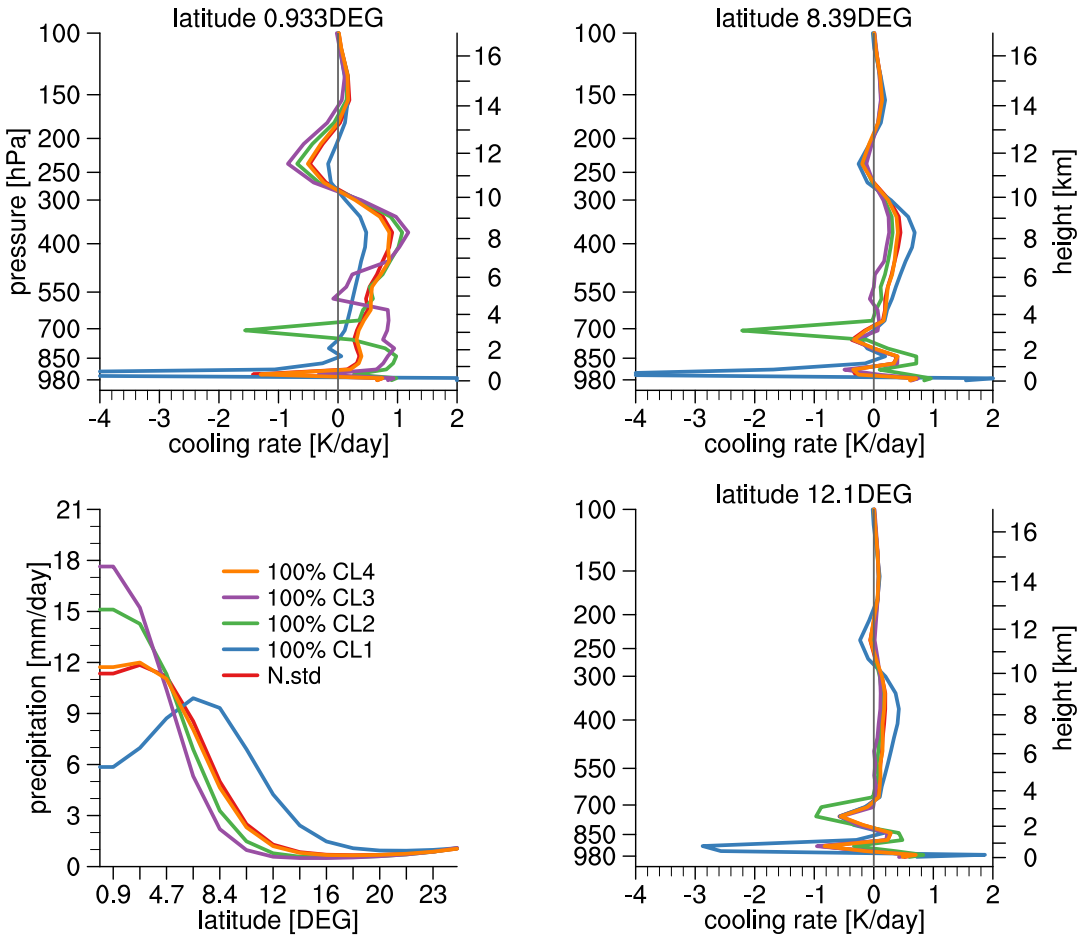


Figure 7.4: Time and zonal average precipitation and cloud longwave radiative effect cooling rates for the 100% CL1-4 and N.std experiments.

the freezing level at about 580 hPa and has a typical cloud cover of 7%. However CL3 is only observed in case of a single ITCZ. CL4 is a ice cloud which is mainly located at the ITCZ and created by the cloud top detrainment of deep convection. Unlike the other three clouds CL4 is relatively widely vertically spread between about 420 hPa and 220 hPa and has a typical time average cloud cover which increases with height from 10% at 420 hPa up to 50% at 150 hPa. However the events which actually have non zero ice for a model grid cell in the CL4 region a typical cloud cover close to 100%. For N.std there is strong cooling through the cloud radiative effect at the height of CL1 which is stronger at the ITCZ than off it (Figure 7.1). Nevertheless this cooling is just below the lower troposphere and thus should not have a strong influence on the ITCZ

position. Above CL1 up to 300 hPa there is strong heating through the cloud radiative effect at the ITCZ in N.std which gets weaker off the ITCZ as well as there is strong cooling off the ITCZ at the height of the CL2 cloud. On average there is an on-off ITCZ cooling rate difference in the lower troposphere through the total cloud radiative effect with less cooling, respectively more heating at the ITCZ than off it. Therefore the overall cloud radiative effect should strengthen the on-off ITCZ humidity difference and thus should support the humidity entrainment effect by pushing the ITCZ towards the equator like the water vapor radiative effect does.

To test the influence of the cloud radiative effect on the ITCZ position several experiments are performed with the configuration of N.std experiment except that the input to the radiative transfer scheme is modified for one of the four cloud types, respectively for the model levels as indicated by the hybrid level column in Table 7.1. For the first four experiments the cloud cover is set to 100% for one of the cloud types, thus the present liquid water and ice is homogeneously spread over the model grid cell in the layers of the respective cloud type for the purpose of the radiative transfer calculation. These experiments are named "100% CL$n$" and their results are shown in Figure 7.4. Four further experiments the ice and liquid water mixing ratio is set to zero for one of the cloud types. These experiments are named "0% CL$n$". For the last four experiments the ice and liquid water mixing ratio is multiplied by a factor of two. These experiments are named "2* CL$n$". Some of the "0% CL$n$" and "2* CL$n$" experiments are shown in Figure 7.5. The "0% CL$n$" and "2* CL$n$" experiments which are not shown in Figure 7.5 are those which only insignificantly diverge from N.std.

All four cloud types are quite opaque in N.std and thus the doubling of the mixing ratios in the "2* CL$n$" experiments can not significantly increase the cloud radiative effect. Only the 2* CL4 experiment show a slightly different ITCZ pattern compared to the N.std experiment. Therefore in the 100% CL$n$ experiments the opacity of the clouds is only slightly reduced through the homogeneous distribution of the liquid and ice over the whole gridpoint while the highly increased cloud cover significantly increases the cloud radiative effect compared to the low cloud cover rates of the N.std experiment, except the 100% CL4 experiment which shows a ITCZ pattern almost similar to the N.std since the actual cloud cover is already close to 100% in N.std anyway. In the 100% CL1 experiment the cooling by the cloud radiative effect just above the height of this cloud is greatly increased while the heating below is also increased. Further the heating above CL1 up to 300 hPa is reduced since the CL1 cloud partly shields the free troposphere from the surface longwave radiation weakening the effect of CL2, CL3 and CL4 cloud which weakens the on-off ITCZ cooling rate difference in the lower troposphere leading to an shift of the ITCZ off the equator in 100% CL1 compared to N.std. In the 100% CL2 experiment there is more cooling by the cloud radiative effect above the position of the CL2 cloud (770 hPa) and increased heating below compared to N.std. The increased cooling is more emphasized off the ITCZ while the increased

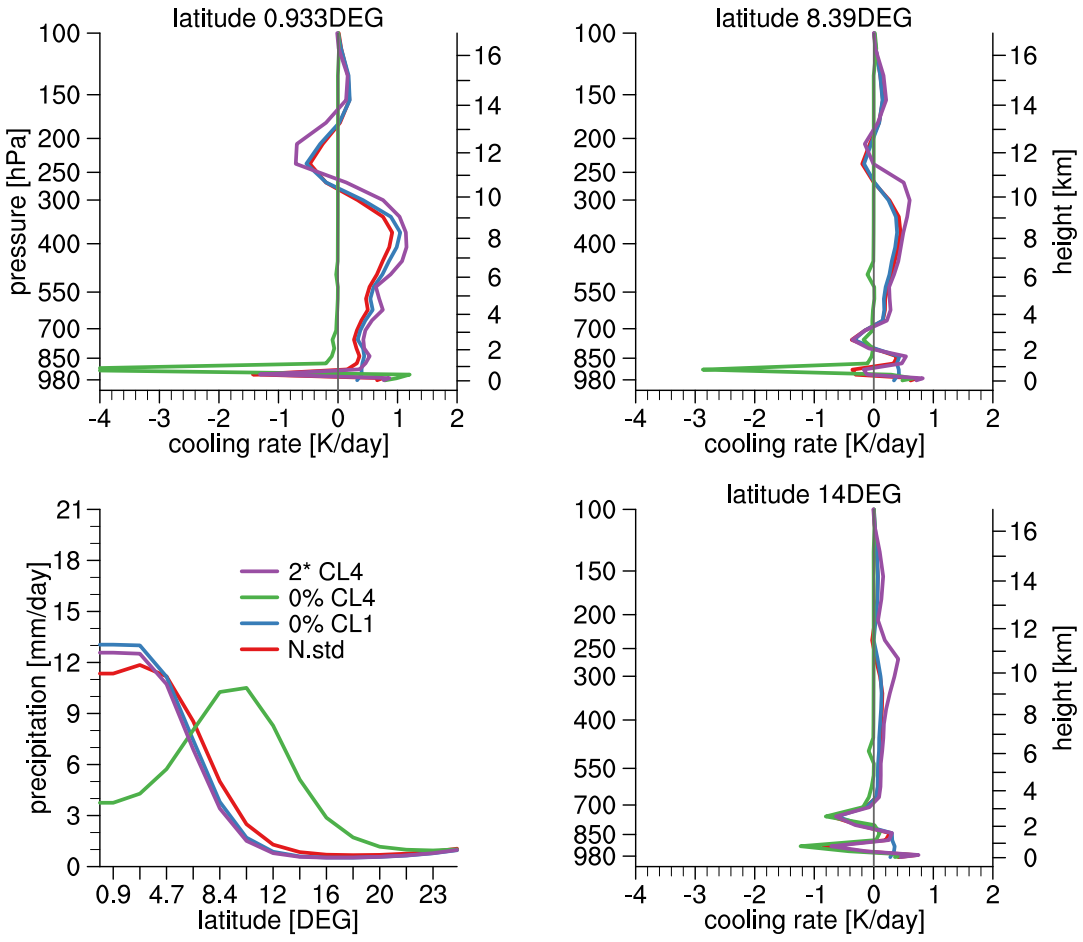


Figure 7.5: Time and zonal average precipitation and cloud longwave radiative effect cooling rates for the 2 CL4, 0% CL4, 0% CL1 and N.std experiments.

heating is more emphasized at the ITCZ strengthening the on-off ITCZ cooling rate difference in the lower troposphere leading to a stronger peaking of the ITCZ around the equator compared to N.std as expected from the humidity entrainment feedback. In the 100% CL3 experiment there is more heating through the cloud radiative effect in the lower troposphere and less heating above at the ITCZ compared to N.std, while heating off the ITCZ by the cloud radiative effect is almost similar compared to N.std, since the CL3 cloud is limited to the ITCZ region. Also in the 100% CL3 experiment the on-off ITCZ cooling rate difference in the lower troposphere is strengthened compared to N.std and the ITCZ is stronger peaked around the equator compared to N.std. The 0% CL2 and 0% CL3 experiment show a ITCZ pattern almost similar to N.std (not

shown), since due to their low cloud cover the cloud radiative effect from the CL2 and CL3 cloud in N.std is small anyway. Even though the cloud cover is is not large for the CL1 cloud in N.std its removal in 0% CL1 let more surface longwave radiation enter the free troposphere and thus strengthen the effect of the other three cloud types and thus leads to a slightly stronger peaking of the ITCZ around the equator compared to N.std. Due to its main location in the ITCZ region, its high cloud cover and opacity as well as its position above the lower troposphere the CL4 cloud is responsible for the vast majority of the cloud radiative effect as well as the on-off ITCZ heating rate difference in the lower troposphere through the cloud radiative effect. Thus it is no surprise that the whole cloud radiative effect is almost zero in the 0% CL4 experiment expect the cooling by the CL1 cloud and some very weak signals by CL2 and CL3. The absence of the on-off ITCZ heating rate difference by the cloud radiative effect in the 0% CL4 experiment weakens the humidity entrainment effect and leads to a large shift of the ITCZ in poleward direction compared to N.std.

In summary the cloud radiative effect of CL1, CL2 and CL3 cloud is limited by their low cloud cover. While all four cloud types are relative opaque thus a scaling of the liquid and ice mixing ratios show a weak influence on the cloud radiative effect. The CL1 cloud partly shields free troposphere from the surface longwave radiation and thus weakens the radiative effect of the other three clouds. Due to its location in the middle of the lower troposphere the CL2 cloud cools the upper lower troposphere and heats the lower lower troposphere. Over all the cooling of the CL2 cloud dominates and its main occurrence outside the ITCZ leads to a strengthening of the on-off ITCZ heating rate difference by the CL2 cloud. Its position on top of the lower troposphere leads to a heating of the lower troposphere by the CL3 cloud and its predominant occurrence at the ITCZ strengthens the on-off ITCZ heating rate difference. Finally the CL4 cloud dominates the total cloud radiative effect and the on-off ITCZ heating rate difference by the cloud radiative effect and thus is a crucial factor for the humidity entrainment effect to push the ITCZ towards the equator similar as the water vapor radiative effect.

# Chapter 8

# Conclusion

For a given distribution of boundary forcings two different convection schemes, as here represented by the original Tiedtke scheme and the modifications introduced by Nordeng for the case of deep convection, can lead to large differences in the position and structure of the inter tropical convergence zone (ITCZ). Depending on assumptions made in the convection scheme, a double ITCZ can result even with the sea surface temperature maximum located at the equator. As near equatorial sea surface temperature gradients become smaller, and the equatorial sea surface temperature maximum becomes less pronounced, convection preferentially locates away from the equator, but to a degree that depends on the details of the deep convection parameterization.

Our results suggest that the distribution of boundary layer moist static energy is key to understanding the placement of the ITCZ. Boundary layer moist static energy is not directly bound to the sea surface temperature profile but strongly depends on the low level wind profile. As a result, the moist static energy maximum in the planetary boundary layer (and hence convection) can be located off the equator even with the sea surface temperature maximum at the equator. By prescribing the windspeed input into the surface heat flux scheme it is possible to control the boundary layer moist static energy, and the placement of convection, irrespective of the distribution of sea surface temperatures.

The sensitivity of the convection to the boundary layer moist static energy follows from its influence, through the updraft model, on the cloud top height. Additional factors influencing cloud top height include the lapse rate of the updraft as a function of mixing rates and (at least for non adiabatic updraft models) environmental humidity and the virtual temperature profile of the free troposphere. Although the latter depends on the former through the action of convection. As a result the ITCZ position is controlled by a feedback loop in which off equatorial deep convection decreases the low level winds in the equatorward direction (the doldrums), reducing the surface evaporation and thus the moist static energy. As the moist static energy in the boundary layer is decreasing close to the equator, even if the surface moist static energy is increasing, its maximum moves in the direction of stronger winds, i.e., the poleward direction and brings the convection and the ITCZ along with it. This mechanism is sufficiently effec-

tive in lowering the moist static energy maximum in the boundary layer, to allow the free tropospheric temperature to cool, which allows for even more off equatorial deep convection. The feedback loop is effective in driving the ITCZ off the equator only if the meridional sea surface temperature gradients are sufficiently weak, otherwise the moist static energy close to the equator can not be decreased strong enough by decreasing low level winds.

The balance of this feedback loop also depends on the updraft mixing rates. If all other things are equal, whether or not shallow or deep convection forms strongly depends on the humidity of the free troposphere, at least in the case when the updraft mixing rates are sufficiently large. For a double ITCZ the moist static energy in the boundary layer is nearly constant in the equatorward direction of the ITCZ while it strongly decreases in the poleward direction. The humidity of the lower troposphere is closely bound to the moist static energy in the boundary layer. The tendency for the humidity in the lower free troposphere to be higher on the equatorward side of a double ITCZ favors convection in this region, particularly for convective parameterizations that have a strongly mixing updraft model, and thus are sensitive to free tropospheric humidity. Also, the time and zonal structure of the ITCZ depends on the mixing rates within the updraft model. Strongly mixing updrafts tend to produce more intermittent convection and more organized convective features.

The convective organization of the feedback loop depends on intensifying deep convection at the ITCZ through a moist free troposphere and suppressing deep convection off the ITCZ through a dry free troposphere. The on to off ITCZ humidity difference needed for the convective organization is build by large scale updrafts at the ITCZ through strong convective heating and large scale subsidence off the ITCZ by prevailing longwave radiative cooling. Nevertheless the convective heating difference is not sufficient to push the feedback loop but it must be supported by a longwave radiative cooling difference which is once driven by the water vapor contrast and second by the radiative effect of the ice cloud anvil produced by the deep updrafts.

An idealized setup of the Tiedtke scheme proofed that an increase of the mixing rates leads to a shift of the ITCZ towards the equator. Thereby the mixing in the upper part of the free troposphere has nearly no influence on the ITCZ placement while a sufficient amount of mixing is needed through the whole lower free troposphere in order to decrease the updraft moist static energy close enough to the environmental saturated moist static energy, which has a minimum in the middle of the free troposphere, such that the variability of those two quantities can influence the updraft height, such that the updraft height not only depends on the convective trigger and boundary layer moist static energy. Vertical inhomogeneous mixing rate profiles show a a quite complex influence on the ITCZ position and need further research.

The present study identified the mechanism through which the entrainment rates influence the ITCZ position, but this mechanism strongly depends on the efficiency

of gravity waves in equalizing the thermal structure of the free troposphere, hence for sea surface temperature maxima further away from the equator the higher Coriolis force should modify the mechanism like in Chao and Chen (2001). Therefore this study should be expanded on sea surface temperature profiles with a off equatorial maximum. This study mainly analyzes the entrainment effect the ITCZ position, nevertheless it was also shown that the entrainment has also a influence on the wave-activity, as shown by the Hovmöller diagrams (Figure 4.3). Thus further research should analyze the entrainment influence on other phenomena than the ITCZ position which also depend on convective organization like the wave spectrum. Finally further research should also test how strong the entrainment humidity feedback is in a full GCM compared to other effects which influence the ITCZ placement there, like the land-sea distribution.

# Bibliography


Arakawa, A. and W. H. Schubert, 1974: Interaction of a cumulus cloud ensemble with the large-scale environment, part i. *J. Atmos. Sci.*, **31**, 674–701.

Back, L. E. and C. S. Bretherton, 2009: On the relationship between SST gradients, boundary layer winds, and convergence over the tropical oceans. *J. Clim.*, **22**, 4182–4196, doi:10.1175/2009JCLI2392.1.

Bechtold, P., M. Köhler, T. Jung, F. Doblas-Reyes, M. Leutbecher, M. J. Rodwell, F. Vitart, and G. Balsamo, 2008: Advances in simulating atmospheric variability with the ECMWF model: From synoptic to decadel time-scales. *Q. J. R. Meteorol. Soc.*, **134**, 1337–1351,doi:10.1175/2009JCLI2392.1.

Bellon, G. and A. H. Sobel, 2010: Multiple equilibria of the Hadley circulation in an intermediate-complexity axisymmetric model. *J. Clim.*, **23**, 1760–1778, doi:10.1175/2009JCLI3105.1.

Bretherton, C. S., M. E. Peters, and L. E. Back, 2004: Relationships between water vapor path and precipitation over the tropical oceans. *J. Clim.*, **17**, 1517–1528.

Chao, W. C. and B. Chen, 2001: Multiple quasi equilibria of the ITCZ and the origin of monsoon onset. part ii: Rotational ITCZ attractors. *J. Atmos. Sci.*, **58**, 2820–2831.

Chao, W. C. and B. Chen, 2004: Single and double ITCZ in an aqua-planet model with constant sea surface temperature and solar angle. *Clim. Dyn.*, **22**, 447–459, doi:10.1007/s00382-003-0387-4.

Charney, J. G., 1971: Tropical cyclogenesis and the formation of the intertropical convergence zone. *Mathematical Problems of the Geophysical Fluid Dynamics*, W. H. Reid, Ed., Am. Math. Soc., Vol. 13, 355–368.

Derbyshire, S. H., I. Beau, P. Bechtold, J.-Y. Grandpeix, J.-M. Piriou, J.-L. Redelsperger, and P. M. M. Soares, 2004: Sensitivity of moist convection to environmental humidity. *Q. J. R. Meteorol. Soc.*, **130 (604)**, 3055–3079, doi:10.1256/qj.03.130.

Emanuel, K. A., 1987: An air-sea interaction model of intraseasonal oscillations in the tropics. *J. Atmos. Sci.*, **44 (16)**, 2324–2340.

Emanuel, K. A., J. D. Neelin, and C. S. Bretherton, 1994: On large-scale circulations in convecting atmospheres. *Q. J. R. Meteorol. Soc.*, **120 (519)**, 1111–1143.

Hess, P. G., D. S. Battisti, and P. J. Rasch, 1993: Maintenance of the intertropical convergence zone and the large-scale tropical circulation on a water-covered earth. *J. Atmos. Sci.*, **50 (5)**, 691.

Holloway, C. E. and J. D. Neelin, 2009: Moisture vertical structure, column water vapor, and tropical deep convection. *J. Atmos. Sci.*, **66 (6)**, 1665–1683, doi:10.1175/2008JAS2806.1.

Holton, J. R., J. M. Wallace, and J. A. Young, 1971: On the boundary layer dynamics and the ITCZ. *J. Atmos. Sci.*, **28**, 275–280.

Hyashi, Y.-Y. and A. Sumi, 1986: The 30-40 day oscillation simulated in an "aqua planet" model. *J. Meteorol. Soc. Jpn.*, **64 (4)**, 451–467.

Johnson, R. H., M. Rickenbach, S. A. Rutledge, P. E. Ciesielski, and W. H. Schubert, 1999: Trimodal characteristics of tropical convection. *J. Clim.*, **12**, 2397–2418.

Lee, M.-I., I.-S. Kang, and B. E. Mapes, 2003: Impacts of cumulus convection parameterization on aqua-planet AGCM simulations of tropical intraseasonal variability. *J. Meteorol. Soc. Jpn.*, **81 (5)**, 963–992.

Lin, J.-L., 2007: The double-ITCZ problem in IPCC ar4 coupled GCMs: Ocean–atmosphere feedback analysis. *J. Clim.*, **20**, 4497–4525, doi:10.1175/JCLI4272.1.

Lindzen, R. S. and S. Nigam, 1987: On the role of sea surface temperature gradients in forcing low-level winds and convergence in the tropics. *J. Atmos. Sci.*, **44 (17)**, 2418–2436.

Liu, Y., L. Guo, G. Wu, and Z. Wang, 2009: Sensitivity of ITCZ configuration to cumulus convective parameterizations on an aqua planet. *Clim. Dyn.*, online, doi:10.1007/s00382-009-0652-2.

Mauritsen, T., et al., 2012: Tuning the climate of a global model. *J. Adv. Model. Earth Syst.*, in press.

Medeiros, B., B. Stevens, I. M. Held, M. Zhao, D. L. Williamson, J. G. Olson, and C. S. Bretherton, 2008: Aquaplanets, climate sensitivity, and low clouds. *J. Clim.*, **21 (19)**, 4974–4991, doi:10.1175/2008JCLI1995.1.

Meehl, G. A., C. Covey, K. E. Taylor, T. Delworth, R. J. Stouffer, M. Latif, and B. McAvaney, 2007: The WCRP CMIP3 multimodel dataset: A new era in climate change research. *Bull. Am. Meteorol. Soc.*, **88(9)**, 1383–1394, doi:10.1175/BAMS-88-9-1383.

Möbis, B., B. Stevens, 2012: Factors controlling the position of the Intertropical Convergence Zone on an aquaplanet. *J. Adv. Model. Earth Syst.*, **4**, M00A04, doi:10.1029/2012MS000199.

Neale, R. B. and B. J. Hoskins, 2001: A standard test for AGCMs including their physical parameterizations: I: The proposal. *Atmospheric Science Letters*, **1**, 7.

Neale, R. B., J. H. Richter, and M. . Jochum, 2008: The impact of convection on ENSO: From a delayed oscillator to a series of events. *J. Clim.*, **21**, 5904–5924, doi:10.1175/2008JCLI2244.1.

Neelin, J. D. and I. M. Held, 1987: Modeling tropical convergence based on the moist static energy budget. *Mon. Weather Rev.*, **115**, 3–12.

Neelin, J. D., O. Peters, and K. Hales, 2009: The transition to strong convection. *J. Atmos. Sci.*, **66**, 2367–2384, doi:10.1175/2009JAS2962.1.

Nordeng, T. E., 1994: Extended versions of the convective parameterization scheme at ECMWF and their impact on the mean transient activity of the model in the tropics. Tech. Memo. 206, ECMWF, Reading, UK.

Nuijens, L., B. Stevens, and A. P. Siebesma, 2009: The environment of precipitating shallow cumulus convection. *J. Atmos. Sci.*, **66 (7)**, 1962–1979, doi:10.1175/2008JAS2841.1.

Numaguti, A., 1993: Dynamics and energy balance of the Hadley circulation and the tropical precipitation zones: Significance of the distribution of evaporation. *J. Atmos. Sci.*, **50 (13)**, 1874–1887.

Numaguti, A. and Y. Hayashi, 1991: Behavior of cumulus activity and the structures of circulations in an "aquaplanet" model part ii: Eastward-moving planetary scale structure and the intertropical convergence zone. *J. Meteorol. Soc. Jpn.*, **69 (5)**, 563–579.

Oueslati, B. and G. Bellon, 2012: Tropical precipitation regimes and mechanisms of regime transitions : contrasting two aquaplanet general circulation models. *Clim. Dyn.*, online, doi:10.1007/s00382-012-1344-x.

Prive, N. C. and R. A. Plumb, 2007: Monsoon dynamics with interactive forcing. part I: Axisymmetric studies. *J. Atmos. Sci.*, **64**, 1417–1430, doi:10.1175/JAS3916.1.

Raymond, D. J., G. B. Raga, C. S. Bretherton, J. Molinari, C. López-Carrillo, and Ž. Fuchs, 2003: Convective forcing in the intertropical convergence zone of the eastern pacific. *J. Atmos. Sci.*, **60**, 2064–2082, doi:10.1175/1520-0469(2003)060¡2064:CFITIC¿2.0.CO;2.

Raymond, D. J., S. L. Sessions, A. H. Sobel, and Ž. Fuchs, 2009: The mechanics of gross moist stability. *J. Adv. Model. Earth Syst.*, **2**, doi:10.3894/JAMES.2009.1.9.

de Rooy, W. C., P. Bechtold, K. Fröhlich, C. Hohenegger, H. Jonker, D. Mironov, A. P. Siebesma, J. Teixeira, and J. Yano, 2012: Entrainment and detrainment in cumulus convection: An overview. *Q. J. R. Meteorol. Soc.*, doi:10.1002/qj.1959.

Sobel, A. H. and J. D. Neelin, 2006: The boundary layer contribution to intertropical convergence zones in the quasi-equilibrium tropical circulation model framework. *Theor. Comput. Fluid Dyn.*, **20 (5-6)**, 323–350, doi:10.1007/s00162-006-0033-y.

Stevens, B., 2006: Bulk boundary-layer concepts for simplified models of tropical dynamics. *Theor. Comput. Fluid Dyn.*, **20 (5-6)**, 279–304, doi:10.1007/s00162-006-0032-z.

Stevens, B., et al., 2012: The atmospheric component of the MPI-M Earth: ECHAM6. *J. Adv. Model. Earth Syst.*, submitted.

Tiedtke, M., 1989: A comprehensive mass flux scheme for cumulus parameterization in large-scale models. *Mon. Weather Rev.*, **117**, 1779–1800.

Tompkins, A. M., 2001: Organization of tropical convection in low vertical wind shears: The role of water vapor. *J. Atmos. Sci.*, **58**, 529–545.

Williamson, D. L., 2008: Convergence of aqua-planet simulations with increasing resolution in the community atmospheric model, version 3. *Tellus, Ser. A*, **60 (5)**, 848–862, doi:10.1111/j.1600-0870.2008.00339.x.

Williamson, D. L., 2012: Ape atlas. Technical note, NCAR, http://www.met.reading.ac.uk/ mike/APE/atlas.html.

# Acknowledgements

First I want to thank my supervisor Bjorn Stevens for his patience, support and guidance throughout my whole PhD time and especially for granting me as much scientific freedom as possible. I further want to thank Marco Giorgetta, Cathy Hohenegger, Traute Crüger and many others for fruitful scientific discussions and various support throughout my PhD time at the MPI-M. I also want to thank the whole atmosphere department for providing the ever stimulating and collegial research environment.

This research was made possible through the support of the Max Planck Society for the Advancement of Science and the German Climate Computing Center (DKRZ), Hamburg. The research leading to these results has received funding from the European Union, Seventh Framework Program (FP7/2007-2013) under grant agreement no 244067.



ISSN 1614-1199